Förster resonance energy transfer rate in any dielectric nanophotonic medium with weak dispersion

2016 New J. Phys. 18 053037

(http://iopscience.iop.org/1367-2630/18/5/053037)

New Journal of Physics
The open access journal at the forefront of physics

Deutsche Physikalische Gesellschaft DPG
IOP Institute of Physics

Published in partnership with: Deutsche Physikalische Gesellschaft and the Institute of Physics

OPEN ACCESS

RECEIVED
4 March 2016

REVISED
26 April 2016

ACCEPTED FOR PUBLICATION
27 April 2016

PUBLISHED
26 May 2016

PAPER

Förster resonance energy transfer rate in any dielectric nanophotonic medium with weak dispersion

Martijn Wubs[1,4] **and Willem L Vos**[2,3]

[1] DTU Fotonik, Department of Photonics Engineering, Technical University of Denmark, DK-2800 Kgs. Lyngby, Denmark
[2] Complex Photonic Systems (COPS), MESA+ Institute for Nanotechnology, University of Twente, PO Box 217, 7500 AE Enschede, The Netherlands
[3] www.photonicbandgaps.com
[4] Author to whom any correspondence should be addressed.

E-mail: mwubs@fotonik.dtu.dk **and** w.l.vos@utwente.nl

Keywords: Förster resonance energy transfer (FRET), local optical density of states, nanophotonics, electromagnetic Green tensor

Abstract

Motivated by the ongoing debate about nanophotonic control of Förster resonance energy transfer (FRET), notably by the local density of optical states (LDOS), we study FRET and spontaneous emission in arbitrary nanophotonic media with weak dispersion and weak absorption in the frequency overlap range of donor and acceptor. This system allows us to obtain the following two new insights. Firstly, we derive that the FRET rate only depends on the static part of the Green function. Hence, the FRET rate is independent of frequency, in contrast to spontaneous-emission rates and LDOS that are strongly frequency dependent in nanophotonic media. Therefore, the position-dependent FRET rate and the LDOS at the donor transition frequency are completely uncorrelated for any nondispersive medium. Secondly, we derive an exact expression for the FRET rate as a frequency integral of the imaginary part of the Green function. This leads to very accurate approximation for the FRET rate that features the LDOS that is *integrated over a huge bandwidth* ranging from zero frequency to far into the UV. We illustrate these general results for the analytic model system of a pair of ideal dipole emitters—donor and acceptor—in the vicinity of an ideal mirror. We find that the FRET rate is independent of the LDOS at the donor emission frequency. Moreover, we observe that the FRET rate hardly depends on the frequency-integrated LDOS. Nevertheless, the FRET is controlled between inhibition and 4× enhancement at distances close to the mirror, typically a few nm. Finally, we discuss the consequences of our results to applications of Förster resonance energy transfer, for instance in quantum information processing.

1. Introduction

A well-known optical interaction between pairs of quantum emitters—such as excited atoms, ions, molecules, or quantum dots—is Förster resonance energy transfer (FRET). In this process, first identified in a seminal 1948 paper by Förster, one quantum of excitation energy is transferred from a first emitter, called a donor, to a second emitter that is referred to as an acceptor [1]. FRET is the dominant energy transfer mechanism between emitters in nanometer proximity, since the rate has a characteristic $(r_F/r_{da})^6$ distance dependence, with r_F the Förster radius and r_{da} the distance between donor and acceptor. Other means to control a FRET system are traditionally the spectral properties of the coupled emitters—the overlap between the donor's emission spectrum and the acceptor's absorptions spectrum—or the relative orientations of the dipole moments [1, 2]. FRET plays a central role in the photosynthetic apparatus of plants and bacteria [3, 4]. Many applications are based on FRET, ranging from photovoltaics [5, 6], lighting [7–9], to sensing [10] where molecular distances [11, 12], and interactions are probed [13, 14]. FRET is also relevant to the manipulation, storage, and transfer of quantum information [15–20].

Modern nanofabrication techniques have stimulated the relevant question whether Förster transfer can be controlled purely by means of the nanophotonic environment, while leaving the FRET pair geometrically and chemically unchanged. Indeed, theory and experiments have revealed both enhanced and inhibited FRET rates for many different nanophotonic systems, ranging from dielectric systems via plasmonic systems to graphene [21–39]. At the same time, it is well known that the spontaneous-emission rate of a single emitter is controlled by the nanophotonic environment [40–43]. Following Drexhage's pioneering work [40], it was established that the emission rate is directly proportional (no offset) to the local density of optical states (LDOS) that counts the number of photon modes available for emission [41, 42]. Therefore, the natural question arises whether the FRET rate correlates with the spontaneous-emission rate of the donor, hence with the LDOS at the donor emission frequency, in particular, whether the FRET rate is directly proportional to the emission rate and the LDOS.

Strikingly, a variety of dependencies of the FRET rate on the LDOS have been reported over the years, leading to an ongoing debate if, and how the FRET rate depends on the LDOS. In a pioneering study of energy transfer between Eu^{3+}-ions and dye molecules in a metal microcavity, Andrew and Barnes reported that the transfer rate depends linearly on the donor decay rate and thus on the LDOS at the donor emission frequency [21], although there was also a significant offset from linearity. In a seminal theory paper [22], Dung, Knöll, and Welsch found that the FRET rate is generally differently affected by the Green function than the spontaneous emission rate, namely the FRET rate depends on the total Green function between two positions (donor and acceptor), whereas the emission rate depends on the imaginary part of the Green function at twice the same position (donor) that is directly proportional to the LDOS [44]. Dung *et al* also reported approximately linear relations between the energy-transfer rate and the donor-decay rate for certain models in spatial regions similar to Andrew and Barnes' experiments [22]. An experiment on transfer between ions near a dielectric interface reported that the transfer rate is independent of the LDOS, in agreement with qualitative arguments [23]. A study of transfer between Si nanocrystals and erbium ions near a gold film suggested a linear dependence of the transfer rate on the LDOS [24]. In a subsequent study by the same group, the experimental results were modeled with a transfer rate depending on the square of the LDOS [25]. Possible reasons for the disparity between the experimental observations include insufficient control on the donor–acceptor distance, incomplete pairing of every donor to only one acceptor, or cross-talk between neighboring donor–acceptor pairs.

Therefore, the relation between Förster transfer and the LDOS was recently studied using isolated and efficient donor–acceptor pairs with precisely defined distance between donor and acceptor molecules [32]. The LDOS was precisely controlled by positioning the donor–acceptor pairs at well-defined distances to a metallic mirror [40, 42, 45]. The outcome of this experimental study was that the Förster transfer rate is independent on the optical LDOS, in agreement with theoretical considerations based on Green functions [32]. Consequently, the Förster transfer *efficiency* is greatest for a vanishing emission rate, like in a 3D photonic band gap crystal [43]. Similar results were obtained with different light sources (rare-Earth ions), and with different cavities [34, 38]. In [36] the measured dependence of the FRET rate on the LDOS was reported to be weak for single FRET pairs, and recent theoretical work on collective energy transfer supports these results in the dilute limit [37]. On the other hand, a linear relation between the FRET rate and the LDOS was reported in experiments with donors and acceptors at a few nanometers from metal surfaces [35, 39]. In recent theoretical work on metallic nanospheres, approximately linear relationships between FRET and emission rates were numerically found, but only above a certain threshold for the emission rate [33].

Several experimentally relevant geometries and material models have been considered in the theoretical literature: Dung and co-workers studied the energy transfer between pairs of molecules in the vicinity of planar structures and microspheres; the nanostructures were modeled with Drude–Lorentz dielectric functions typical of metals [22]. Reference [26] studied energy transfer between excitons in nanocrystal quantum dots, mediated by metal nanoparticles that were described with an empirical metallic dielectric function. Reference [29] considered FRET near a metal nanosphere with spatial dispersion. Reference [30] studied plasmon-enhanced radiative energy transfer. Reference [33] studied energy transfer in the vicinity of a metallic sphere with an empirical metallic dielectric function. Reference [37] studied energy transfer in the vicinity of a metallic mirror that was described with an empirical metallic dielectric function. Many of these models thus take material dispersion and resonances and loss into account.

A main purpose of the present article is to provide new theoretical insights in FRET and its possible relationship with the LDOS. To this end, we have chosen to study an as simple as possible model system with vanishing dispersion, as this allows us to derive analytical expressions that are not compounded by intricate dispersive or resonant effects. As the starting point, section 2 summarizes essential expressions of energy-transfer and spontaneous-emission rates in terms of the Green function for light. In section 3 we argue (and illustrate in section 5) that not all energy transfer is FRET, and that the FRET rate is related to only the longitudinal part of the Green function, while the full Green function describes the *total* energy transfer. We derive that the FRET rate becomes strictly frequency-independent, while it is well known that the LDOS is

typically strongly frequency dependent. This general result still leaves open the possibility that the FRET rate depends on the frequency-integrated LDOS (allowing for controlled engineering), an intriguing possibility that has not been explored in the literature to date. Indeed, in section 4 we derive that the FRET rate can be expressed as a frequency integral of the LDOS. In section 5 we test and illustrate our general results for a donor–acceptor pair close to an ideal mirror, a model system that allows analytical expressions both for emission and for energy transfer rates. We notably verify the importance of the broadband LDOS integral. In section 6 we discuss experimental implications of our results. We summarize in section 7, and give a number of derivations in the Appendices.

2. Energy transfer, emission, and Green function

The total energy transfer rate γ_{da} between a donor and an acceptor dipole in any nanophotonic environment is given by

$$\gamma_{da} = \int_{-\infty}^{\infty} \mathrm{d}\omega\ \sigma_a(\omega) w(\mathbf{r}_a, \mathbf{r}_d, \omega) \sigma_d(\omega), \tag{1}$$

where $\sigma_{d,a}(\omega)$ are the donor (single-photon) emission and acceptor (single-photon) absorption spectra in free space [22, 46]. All effects of the nanophotonic environment are contained in the transfer amplitude squared $w(\mathbf{r}_a, \mathbf{r}_d, \omega)$ that can be expressed in terms of the Green function $\mathbf{G}(\mathbf{r}_a, \mathbf{r}_d, \omega)$ of the medium, and the donor and acceptor dipole moments $\boldsymbol{\mu}_d$, $\boldsymbol{\mu}_a$ respectively, as

$$w(\mathbf{r}_a, \mathbf{r}_d, \omega) = \frac{2\pi}{\hbar^2}\left(\frac{\omega^2}{\varepsilon_0 c^2}\right)^2 |\boldsymbol{\mu}_a^* \cdot \mathbf{G}(\mathbf{r}_a, \mathbf{r}_d, \omega) \cdot \boldsymbol{\mu}_d|^2. \tag{2}$$

These expressions for the total energy transfer rate were originally derived by Dung, Knöll, and Welsch for a general class of nanophotonic media that may exhibit both frequency-dispersion and absorption[5] [22]. For homogeneous media, see also [47]. Since we are in this paper interested in FRET, we discuss in section 3 the relation between total energy transfer and FRET.

For the energy transfer rate equation (1) we only need to know the Green function in the frequency interval where the donor and acceptor spectra overlap appreciably. For very broad cases that we are aware of, the overlap bandwidth amounts to 40 nm, or less than 10% relative bandwidth compared to the visible spectral range. For generic dielectric media that show little absorption and weak dispersion in the visible range (see examples in [48]), it is safe to assume that in this relatively narrow frequency overlap interval both absorption and dispersion are sufficiently weak to be neglected. Also, in the experiments of [32], the overlap region was a factor of 10 narrower than the visible spectrum. To model FRET in such weakly dispersive media, we can therefore approximate $\varepsilon(\mathbf{r}, \omega)$ by a real-valued frequency-independent dielectric function $\varepsilon(\mathbf{r})$. The corresponding Green function $\mathbf{G}(\mathbf{r}, \mathbf{r}', \omega)$ is the solution of the usual wave equation for light

$$-\nabla \times \nabla \times \mathbf{G}(\mathbf{r}, \mathbf{r}', \omega) + \varepsilon(\mathbf{r})\left(\frac{\omega}{c}\right)^2 \mathbf{G}(\mathbf{r}, \mathbf{r}', \omega) = \delta(\mathbf{r} - \mathbf{r}')\mathbf{I}, \tag{3}$$

with a localized source on the right-hand side[6]. Unlike $\varepsilon(\mathbf{r})$, the Green function $\mathbf{G}(\mathbf{r}, \mathbf{r}', \omega)$ is frequency-dependent and complex-valued.

While the energy transfer rate in equation (1) evidently depends on the donor and acceptor spectra $\sigma_d(\omega)$ and $\sigma_a(\omega)$, we focus here on the dependence on the environment as given in equation (2). We assume that the donor and acceptor overlap in a range that is sufficiently narrow that the transfer amplitude $w(\mathbf{r}_a, \mathbf{r}_d, \omega)$ varies negligibly in this range. With this assumption we obtain for the energy-transfer rate

$$\bar{\gamma}_{da} = w(\mathbf{r}_a, \mathbf{r}_d, \omega_{da}) \int_{-\infty}^{\infty} \mathrm{d}\omega\ \sigma_a(\omega)\sigma_d(\omega), \tag{4}$$

where ω_{da} is the frequency where the integrand in the overlap integral assumes its maximal value. The overlap integral is the same for *any* nanophotonic environment, so that the ratio of energy transfer rates in two different environments simply depends on the ratio of $w(\mathbf{r}_a, \mathbf{r}_d, \omega_{da})$ in both environments.

Spontaneous emission of the donor is a process that competes with the energy transfer to the acceptor. In the absence of an acceptor molecule, it is well known that the spontaneous emission of the donor in a photonic environment depends on frequency and on position, often described in terms of a local density of states (LDOS). Nowadays, extensive experimental know-how is available on how to engineer the LDOS and thereby the spontaneous-emission rate. Relevant LDOS variations occur near dielectric interfaces and in photonic crystals,

[5] Our function w is the same as $\tilde{w}$ in [22], equation (44).

[6] Our definition of the Green function agrees with [49, 64] and differs by a minus sign from [22, 44].

Table 1. Symbols for the various energy transfer and emission rates used in this paper, with their defining equations.

Glossary of transfer and emission rates	
γ_{da}	Total donor–acceptor energy transfer rate, equation (1)
$\bar{\gamma}_{da}$	Narrowband approximation of transfer rate, equation (4)
γ_{se}	Spontaneous emission rate of the donor, equation (5)
γ_F	Exact FRET rate from donor to acceptor, equation (13)
$\gamma_F^{(L)}$	Broadband LDOS approximated FRET rate, equation (18)
$\bar{\gamma}_F^{(HF)}$	High-frequency approximated FRET rate, equation (23)

for example. An important experimental question is therefore whether the donor–acceptor FRET rate can be controlled by changing the donor-only spontaneous-emission rate [21, 32, 34].

The donor-only spontaneous-emission rate $\gamma_{se}(\mathbf{r}, \omega_d)$ at position $\mathbf{r}$ with real-valued dipole moment $\boldsymbol{\mu} = \mu\hat{\boldsymbol{\mu}}$ and transition frequency ω_d can be expressed in terms of the imaginary part of the Green function of the medium as

$$\gamma_{se}(\mathbf{r}_d, \omega_d) = -\left(\frac{2\omega_d^2}{\hbar\varepsilon_0 c^2}\right)\boldsymbol{\mu}\cdot \mathrm{Im}[\mathbf{G}(\mathbf{r}_d, \mathbf{r}_d, \omega_d)]\cdot\boldsymbol{\mu} \tag{5}$$

or $\gamma(\mathbf{r}_d, \omega_d, \boldsymbol{\mu}) = \pi\mu^2\omega_d\rho_p(\mathbf{r}_d, \omega_d, \hat{\boldsymbol{\mu}})/(3\hbar\varepsilon_0)$ in terms of the partial LDOS

$$\rho_p(\mathbf{r}_d, \omega_d, \hat{\boldsymbol{\mu}}) = -(6\omega_d/\pi c^2)\hat{\boldsymbol{\mu}}\cdot \mathrm{Im}[\mathbf{G}(\mathbf{r}_d, \mathbf{r}_d, \omega_d)]\cdot\hat{\boldsymbol{\mu}}, \tag{6}$$

where $\hat{\boldsymbol{\mu}}$ is a dipole-orientation unit vector [41, 44]. The optical density of states (LDOS) is then defined as the dipole-orientation-averaged partial LDOS [44]. Here we do not average over dipole orientations, as we are interested in possible correlations between energy transfer and spontaneous-emission rates for a fixed dipole orientation[7]. In table 1 we summarize all energy-transfer and spontaneous-emission rates that are defined throughout this paper.

3. Contributions to energy transfer

The total energy transfer rate equation (1) for arbitrary donor–acceptor distances is expressed in terms of the Green function of the medium. As is well known, not all energy transfer is Förster energy transfer. For donor–acceptor distances of less than ten nanometers, one refers to Förster transfer. We will derive below that at these distances one does not need the full Green function to describe energy transfer, which will yield important insights into Förster transfer in inhomogeneous media and will simplify calculations of the FRET rate.

For arbitrary nondispersive and non-lossy media, we can express the Green function in terms of the complete set of optical eigenmodes $\mathbf{f}_\lambda$ satisfying the wave equation

$$-\nabla\times\nabla\times\mathbf{f}_\lambda(\mathbf{r}) + \varepsilon(\mathbf{r})(\omega_\lambda/c)^2\mathbf{f}_\lambda(\mathbf{r}) = 0, \tag{7}$$

with positive eigenfrequencies $\omega_\lambda > 0$. The Green function, being the solution of equation (3), can be expanded in terms of these mode functions $\mathbf{f}_\lambda$. An important property of this expansion follows by combining equations (21) and (22) of [49], namely that the Green function can be written as the sum of three terms:

$$\mathbf{G}(\mathbf{r}, \mathbf{r}', \omega) = \underbrace{c^2\sum_\lambda \frac{\mathbf{f}_\lambda(\mathbf{r})\mathbf{f}_\lambda^*(\mathbf{r}')}{(\omega+i\eta)^2-\omega_\lambda^2}}_{\mathbf{G}_R} \underbrace{-\left(\frac{c}{\omega}\right)^2\sum_\lambda \mathbf{f}_\lambda(\mathbf{r})\mathbf{f}_\lambda^*(\mathbf{r}')}_{\mathbf{G}_S} + \frac{(c/\omega)^2}{\varepsilon(\mathbf{r})}\delta(\mathbf{r}-\mathbf{r}')\mathbf{I}. \tag{8}$$

Since the Green function controls the energy transfer rate (see equation (2)), it is relevant to discern energy transfer processes corresponding to these terms. The first term in equation (8) denoted $\mathbf{G}_R$ corresponds to resonant dipole–dipole interaction (RDDI), the radiative process by which the donor at position $\mathbf{r}$ emits a field that is then received by the acceptor at position $\mathbf{r}'$. In case of homogeneous media and only in the far field, this process can be identified with emision and subsequent absorption of transverse photons [51]. Using equation (20) of [49], $\mathbf{G}_R$ can be uniquely identified as the generalized transverse (part of the) Green function of the inhomogeneous medium, with the property that $\nabla\cdot[\varepsilon(\mathbf{r})\mathbf{G}_R(\mathbf{r}, \mathbf{r}', \omega)] = 0$. The name 'resonant' describes that photon energies close to the donor and acceptor resonance energy are the most probable energy transporters, in line with the denominator $(\omega+i\eta)^2 - \omega_\lambda^2$ of this first term.

The second term in equation (8) called $\mathbf{G}_S$ corresponds to the static dipole–dipole interaction (SDDI) that also causes energy transfer from donor to acceptor. The third term in equation (8) is proportional to the Dirac

[7] What is for convenience called LDOS should in the following be understood to be the partial LDOS.

delta function $\delta(\mathbf{r} - \mathbf{r}')$. Since $\mathbf{r} \neq \mathbf{r}'$ in case of energy transfer, this contribution vanishes. Nevertheless, this third term is conceptually also important, since from equation (19) of [49] it follows that the sum of $\mathbf{G}_S$ and the third term can be uniquely identified as the longitudinal (part of the) Green function of the inhomogeneous medium.

In the molecular physics literature, homogeneous environments are typically assumed, and FRET is introduced as a direct consequence of non-retarded Coulombic longitudinal intermolecular interaction [51], and is typically not described in terms of Green functions. Conversely, in the nanophotonic literature, energy transfer in inhomogeneous media is often described in terms of Green functions, but the FRET contribution due to longitudinal interactions is not singled out. The concept of the longitudinal Green function can serve to bridge these two research fields. We identify the longitudinal Green function and hence $\mathbf{G}_S$ to describe the instantaneous electrostatic intermolecular interaction of any inhomogeneous medium[8]. As explained below, it is indeed this SDDI that gives rise to the FRET rate that characteristically scales as r_{da}^{-6} in homogeneous media and dominates the total energy transfer for strongly subwavelength donor–acceptor separations. By identifying the generalized transverse and longitudinal parts of the Green function and relating them to energy transfer processes, we provide a unified theory of radiative and radiationless energy transfer in inhomogeneous dielectrics. Thereby we generalize the pioneering work on energy transfer in homogeneous media by Andrews [51], who demonstrated that radiative and radiationless energy transfer are long-range and short-range limits of the same mechanism.

Equation (8) also provides a practical way of obtaining the static Green function (that controls FRET) from the total Green function, even if a complete set of modes has not been determined. The equation implies that for arbitrary inhomogeneous environments the static part of the Green function is obtained from the total Green function by the following limiting procedure (for $\mathbf{r} \neq \mathbf{r}'$)

$$\mathbf{G}_S(\mathbf{r}, \mathbf{r}', \omega) = \frac{1}{\omega^2} \lim_{\omega \to 0} \omega^2 \mathbf{G}(\mathbf{r}, \mathbf{r}', \omega), \tag{9}$$

which provides a justification of our use of the term 'static'. From equation (9), $\mathbf{G}_S$ appears as the non-retarded near-field approximation of the retarded full Green function. As an important test, selecting in this way the static part of the Green function of a homogeneous medium (A.1) indeed gives that only

$$\mathbf{G}_{h,S}(\mathbf{r}_1, \mathbf{r}_2, \omega) = \frac{c_0^2}{4\pi n^2 \omega^2 r^3}(\mathbf{I} - 3\hat{\mathbf{r}}\hat{\mathbf{r}}), \tag{10}$$

with $\mathbf{r} = \mathbf{r}_1 - \mathbf{r}_2$ contributes to Förster energy transfer, and not the terms of $\mathbf{G}_h$ that vary as $1/r$ and $1/r^2$. This leads to the characteristic FRET rate scaling as $1/r^6$. By contrast, for inhomogeneous media the static Green function not only depends on the distance between donor and emitter, but also on the absolute positions of both donor and acceptor in the medium. In section 5 (figure 2) we will illustrate for one example of such an inhomogeneous medium (near an ideal mirror) that the total energy-transfer rate for donor–acceptor pairs separated by a few nanometers is indeed fully determined by the static Green function as obtained by equation (9). In contrast, this Green function is not of the well-known form (10) for homogeneous media.

Based on the discussion above and without loss of generality we define FRET in inhomogeneous media as that part of the total energy transfer that is mediated by the static Green function. We also define the square of the Förster transfer amplitude, in analogy to equation (2), by

$$w_F(\mathbf{r}_a, \mathbf{r}_d, \omega) \equiv \frac{2\pi}{\hbar^2}\left(\frac{\omega^2}{\varepsilon_0 c^2}\right)^2 |\boldsymbol{\mu}_a^* \cdot \mathbf{G}_S(\mathbf{r}_a, \mathbf{r}_d, \omega) \cdot \boldsymbol{\mu}_d|^2. \tag{11}$$

This equation appears to be similar to equation (2), yet with the total Green function $\mathbf{G}$ replaced by its static part $\mathbf{G}_S$, as defined in equation (8) and computed in equation (9). The FRET rate γ_F is then obtained by substituting $w_F(\mathbf{r}_a, \mathbf{r}_d, \omega)$ for $w(\mathbf{r}_a, \mathbf{r}_d, \omega)$ into equation (1), giving:

$$\gamma_F(\mathbf{r}_a, \mathbf{r}_d) = \int_{-\infty}^{\infty} \mathrm{d}\omega\, \sigma_a(\omega) w_F(\mathbf{r}_a, \mathbf{r}_d, \omega) \sigma_d(\omega). \tag{12}$$

Here we arrive at an important simplification in the description of Förster transfer in inhomogeneous media, by noting that from equations (9) and (11), the quantity $w_F(\mathbf{r}_a, \mathbf{r}_d, \omega)$ is actually *independent of frequency* ω. The FRET rate γ_F is then given by the simple relation

[8] In the minimal-coupling formalism the Hamiltonian features an electrostatic intermolecular interaction that is absent in a multipolar formalism [50], also for inhomogeneous media [52]. Instead, in the multipolar formalism, the electrostatic interaction is an induced interaction that shows up in the Green function [49]. We note that both the RDDI and the SDDI in equation (8) have mode expansions that involve all optical modes, corresponding to arbitrary positive eigenfrequencies ω_λ. The longitudinal Green function and hence $\mathbf{G}_S$ in equation (8) can be expressed in terms of (generalized) transverse mode functions $\mathbf{f}_\lambda$ due to a completeness relation that involves both longitudinal and transverse modes [49].

$$\gamma_{\rm F}(\mathbf{r}_{\rm a}, \mathbf{r}_{\rm d}) = w_{\rm F}(\mathbf{r}_{\rm a}, \mathbf{r}_{\rm d}) \int_{-\infty}^{\infty} {\rm d}\omega\ \sigma_{\rm a}(\omega)\sigma_{\rm d}(\omega). \tag{13}$$

While this expression looks similar to the approximate expression for the total energy transfer rate (equation (4)), we emphasize that equation (13) is an *exact* expression for the FRET rate, also for broad donor and acceptor spectra, valid for *any* photonic environment that is lossless and weakly dispersive in the frequency range where the donor and acceptor spectra overlap. Moreover, the spectral overlap integral in equation (13) is the same for *any* nanophotonic environment[9]. All effects of the nondispersive inhomogeneous environment are therefore contained in the frequency-independent prefactor $w_{\rm F}(\mathbf{r}_{\rm a}, \mathbf{r}_{\rm d})$. In other words, while there is an effect of the nanophotonic environment on the FRET rate as decribed by the medium-dependent static Green function, this effect does not depend on the resonance frequencies of the donor and acceptor (for constant medium-independent overlap integral in equation (13)). But because we have now found that the FRET rate does not depend on the donor and acceptor frequencies, it also follows that the FRET rate can not be a function of the LDOS at these particular frequencies.

4. FRET in terms of a frequency-integrated LDOS

Although the exact expression in equation (13) states that the FRET rate in a nondispersive nanophotonic medium is independent of the LDOS at the donor's resonance frequency, this fact leaves the possibility open that there might be a relation between the FRET rate and a *frequency-integrated* LDOS. We will now derive such a relation, thereby providing a new perspective on efforts to control the FRET rate by engineering the LDOS.

We start with the mode expansion of the Green function in equation (8) to derive a useful new expression, relating the Förster transfer rate to a frequency-integral over ${\rm Im}[\mathbf{G}]$. We use the fact that $\mathbf{G}_{\rm S}(\mathbf{r}, \mathbf{r}', \omega)$ is real-valued, as is proven in [52]. Thus the imaginary part of the Green function is equal to ${\rm Im}[\mathbf{G}_{\rm R}]$ and the mode expansion of ${\rm Im}[\mathbf{G}]$ becomes

$${\rm Im}[\mathbf{G}(\mathbf{r}, \mathbf{r}', \omega)] = -\frac{\pi c^2}{2\omega} \sum_{\lambda} \mathbf{f}_{\lambda}(\mathbf{r}) \mathbf{f}_{\lambda}^{*}(\mathbf{r}') \delta(\omega - \omega_{\lambda}), \tag{14}$$

with $\omega > 0$. We note that only degenerate modes with frequencies $\omega_{\lambda} = \omega$ show up in this mode expansion of ${\rm Im}[\mathbf{G}]$. This can also be seen in another way: the defining equation for the Green function equation (3) implies that the *imaginary* part of the Green function satisfies the same source-free equation (7) as the subset of modes $\mathbf{f}_{\lambda}(\mathbf{r})$ for which the eigenfrequency ω_{λ} equals ω. The mode expansion (14) is indeed a solution of equation (7). Therefore, ${\rm Im}[\mathbf{G}(\mathbf{r}, \mathbf{r}', \omega)]$ and hence the LDOS and the spontaneous-emission rate (equation (5)) can be completely expanded in terms of only those degenerate eigenmodes, in contrast to the energy transfer that requires *all* optical modes, see equation (8).

When we multiply equation (14) by ω and integrate over ω, we obtain as one of our major results an exact identity for the static Green function

$$\mathbf{G}_{\rm S}(\mathbf{r}_{\rm a}, \mathbf{r}_{\rm d}, \omega) = \frac{2}{\pi\omega^2} \int_{0}^{\infty} {\rm d}\omega_1\ \omega_1\ {\rm Im}[\mathbf{G}(\mathbf{r}_{\rm a}, \mathbf{r}_{\rm d}, \omega_1)]. \tag{15}$$

This identity is valid for a general nanophotonic medium in which material dispersion can be neglected. Equation (15) was derived using a complete set of modes, yet does not depend on the specific set of modes used. When inserting this identity into equation (11), we express $w_{\rm F}(\omega)$ and hence the FRET rate $\gamma_{\rm F}$ of equation (12) in terms of an integral over the imaginary part of the Green function. While this is somewhat analogous to the well-known expression for the spontaneous-emission rate equation (5), there are two important differences: the first difference between equation (15) for Förster energy transfer and equation (5) for spontaneous emission in terms of ${\rm Im}[\mathbf{G}]$ is of course that equation (15) is an *integral over all positive frequencies*. The second main difference is that in equation (15) the Green function ${\rm Im}[\mathbf{G}(\mathbf{r}_{\rm a}, \mathbf{r}_{\rm d}, \omega_1)]$ appears with *two* position arguments—one for the donor and one for the acceptor—instead of only one position as in the spontaneous-emission rate. A major advantage of an expression in terms of ${\rm Im}[\mathbf{G}]$ is that ${\rm Im}[\mathbf{G}]$ does not diverge for $\mathbf{r}_{\rm a} \to \mathbf{r}_{\rm d}$, in contrast to ${\rm Re}[\mathbf{G}]$. In appendix C we verify and show explicitly that the identity in equation (15) holds both in homogeneous media as well as for the nanophotonic case of arbitrary positions near an ideal mirror.

We now use equation (15) to derive an approximate expression $\mathbf{G}_{\rm S}^{\rm (L)}$ for the static Green function $\mathbf{G}_{\rm S}$ that allows us to find an interesting relation between the FRET rate and the frequency-integrated LDOS. Our approximation is motivated by the fact that ${\rm Im}[\mathbf{G}(\mathbf{r}_{\rm d} - \mathbf{r}_{\rm a}, \omega)]$ for homogeneous media (based on equation (A.1)) varies appreciably only for variations in the donor–acceptor distance $r_{\rm da}$ on the scale of the wavelength of light, typically $r_{\rm da} \simeq \lambda_0 = 500$ nm (with $\lambda_0 = 2\pi c/\omega_0$). From equation (A.6) it follows that the same holds true for ${\rm Im}[\mathbf{G}(\mathbf{r}_{\rm d}, \mathbf{r}_{\rm a}, \omega)]$ for the ideal mirror. In contrast, FRET occurs on a length scale of

[9] Let us recall here that $\sigma_{\rm a}(\omega)$ and $\sigma_{\rm d}(\omega)$ are the donor's emission spectrum and acceptor's absorption spectrum in *free space*, see equation (1) and [22, 46].

$r_{da} \simeq 5$ nm, typically a hundred times smaller. Motivated by these considerations, we approximate $\mathrm{Im}[\mathbf{G}(\mathbf{r}_a, \mathbf{r}_d, \omega_1)]$ in the integrand of equation (15) by the zeroth-order Taylor approximation $\mathrm{Im}[\mathbf{G}(\mathbf{r}_d, \mathbf{r}_d, \omega_1)]$. The accuracy of this approximation depends on the optical frequency ω. The approximation will therefore not hold for all frequencies that are integrated over, and becomes worse for higher frequencies. But it appears that we can make an accurate approximation throughout a huge optical bandwidth $0 \leqslant \omega_1 \leqslant \Omega$. If we choose $\Omega = 10\omega_0$, i.e, a frequency bandwidth all the way up to the vacuum ultraviolet (VUV), then $\mathrm{Im}[\mathbf{G}(\mathbf{r}_a, \mathbf{r}_d, \omega_1)]$ will only deviate appreciably from $\mathrm{Im}[\mathbf{G}(\mathbf{r}_d, \mathbf{r}_d, \omega_1)]$ for donor–acceptor distances $r_{da} > \lambda_0/10$, which is in practice of the order of 50 nm, much larger than typical donor–acceptor distances in Förster transfer experiments. We obtain the expression for the approximate static Green function $\mathbf{G}_S^{(L)}$ as

$$\mathbf{G}_S^{(L)}(\mathbf{r}_a, \mathbf{r}_d, \omega) = \frac{2}{\pi\omega^2}\int_0^{\Omega} \mathrm{d}\omega_1\, \omega_1\, \mathrm{Im}[\mathbf{G}(\mathbf{r}_d, \mathbf{r}_d, \omega_1)] + \frac{2}{\pi\omega^2}\int_{\Omega}^{\infty} \mathrm{d}\omega_1\, \omega_1\, \mathrm{Im}[\mathbf{G}(\mathbf{r}_a, \mathbf{r}_d, \omega_1)]. \tag{16}$$

The first term of this equation is recognized to be an integral of the LDOS over a large frequency bandwidth, ranging from zero frequency (or 'DC') to a high frequency Ω in the VUV range. While the specific value of Ω does not matter much, it is important that Ω can be chosen much greater than optical frequencies, while the inequality $n(\mathbf{r}_d)\Omega r_{da}/c \ll 1$ still holds. Within this approximation, we can find an expression for the FRET rate for donor and acceptor molecules with parallel (but not necessarily equal) dipole moments, i.e. $\boldsymbol{\mu}_a = \mu_a\hat{\boldsymbol{\mu}}$ and $\boldsymbol{\mu}_b = \mu_b\hat{\boldsymbol{\mu}}$. To this end, we substitute $\mathbf{G}_S$ for $\mathbf{G}_S^{(L)}$ in w_F (equation (11)) and express the imaginary part of the Green function in terms of the partial LDOS ρ_p of equation (6), to obtain a new approximate transfer amplitude squared

$$w_F^{(L)}(\mathbf{r}_a, \mathbf{r}_d) = \frac{8\mu_a^2\mu_b^2}{\pi\varepsilon_0^2\hbar^2c^4}\left|\frac{\pi c^2}{6}\int_0^{\Omega}\mathrm{d}\omega_1\rho_p(\mathbf{r}_d, \omega_1, \hat{\boldsymbol{\mu}}) - \int_{\Omega}^{\infty}\mathrm{d}\omega_1\,\omega_1\,\hat{\boldsymbol{\mu}}\cdot\mathrm{Im}[\mathbf{G}(\mathbf{r}_a, \mathbf{r}_d, \omega_1)]\cdot\hat{\boldsymbol{\mu}}\right|^2. \tag{17}$$

Just like $w_F(\mathbf{r}_a, \mathbf{r}_d)$ in equation (11), its 'LDOS approximation' $w_F^{(L)}(\mathbf{r}_a, \mathbf{r}_d)$ in equation (17) is independent of the donor emission frequency. Substituting w_F in equation (12) with $w_F^{(L)}$, we obtain an approximate[10] FRET rate $\gamma_F^{(L)}$

$$\gamma_F^{(L)} = w_F^{(L)}(\mathbf{r}_a, \mathbf{r}_d)\int_{-\infty}^{\infty}\mathrm{d}\omega\,\sigma_a(\omega)\sigma_d(\omega). \tag{18}$$

The approximate FRET rate $\gamma_F^{(L)}$ thus depends on the LDOS, albeit integrated over a broad frequency range from zero to Ω (equation (17)). In section 5 we will give an example where this approximation is extremely accurate, and we also explore by how much the integrated LDOS controls the FRET rate.

5. Energy transfer near a mirror

As a concrete example of our theoretical considerations, we study energy transfer from a single donor to a single acceptor separated by a distance $r_{da} = |\mathbf{r}_a - \mathbf{r}_d|$ in the vicinity of an ideal mirror. To limit parameter space, we focus on situations in which the donor and the acceptor have the same distance z to the mirror, and where the dipole moments of dipole and acceptor point in the same direction. In the parallel ($\parallel$) configuration shown in figure 1(a), both dipole moments are oriented parallel to the mirror, and the dipoles point normally to the mirror in the perpendicular ($\perp$) configuration of figure 1(b). In general, both the LDOS and the partial LDOS for any dipole orientation are fixed once the partial LDOS is known for nine independent dipole orientations, but for planar systems considered here, the two directions $\perp$ and $\parallel$ suffice for a complete description [53].

For homogeneous media it is well known that Förster energy transfer dominates the total energy transfer at strongly sub-wavelength distances, and we will now see that this is also the case in inhomogeneous media, by means of the ideal mirror. The total energy transfer near an ideal mirror depends on the total Green function as given in equations (A.7) and (A.8) for the two dipole configurations (see figure 1). For the donor and acceptor near the mirror in the parallel configuration, we obtain for the static part

$$\boldsymbol{\mu}^{\parallel}\cdot\mathbf{G}_S(\mathbf{r}_a, \mathbf{r}_d, \omega)\cdot\boldsymbol{\mu}^{\parallel} = \frac{\mu^2c^2}{4\pi n^2\omega^2}\left\{\frac{1}{r_{da}^3} - \frac{1}{(\sqrt{r_{da}^2 + 4z^2})^3}\right\}, \tag{19}$$

[10] In the symbol $\gamma_F^{(L)}$ the superscript L is meant to indicate a FRET rate in terms of the LDOS.

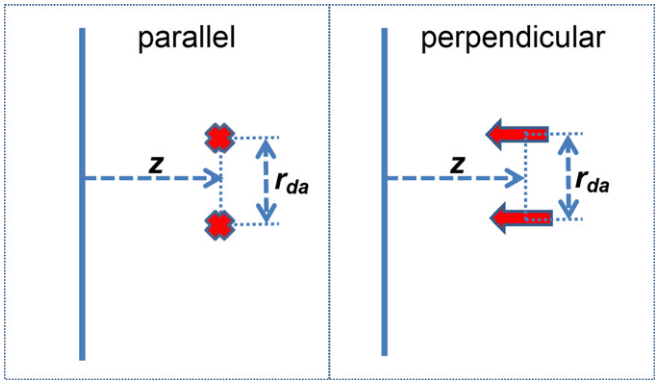

Figure 1. We study pairs of donor and acceptor dipoles that are separated by a distance r_{da}, and located at a distance z from an ideal mirror. We focus on two configurations where the dipoles are oriented perpendicular to the position difference of donor and acceptor $(\hat{\boldsymbol{\mu}}_d, \hat{\boldsymbol{\mu}}_a) \perp (\mathbf{r}_d - \mathbf{r}_a)$: (Left) Both dipole moments of donor and acceptor are parallel to the mirror surface ('parallel configuration', $\|$) and parallel to each other. (Right) Both dipole moments of donor and acceptor are perpendicular to the mirror surface ('perpendicular configuration', $\perp$) and parallel to each other.

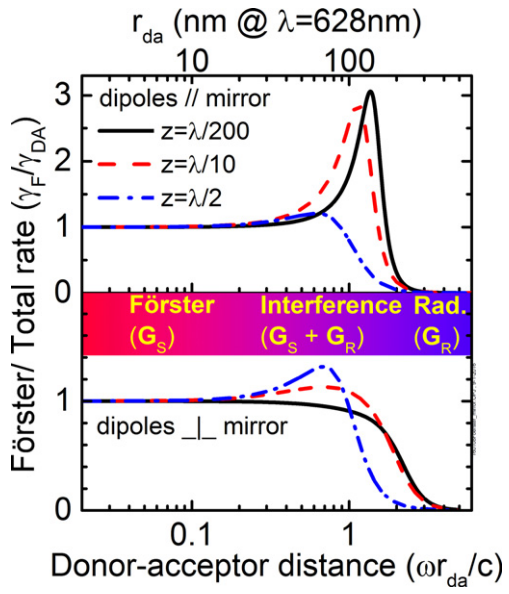

Figure 2. Ratio of the Förster resonance energy transfer rate to the total energy transfer rate (γ_F/γ_{da}) versus donor–acceptor distance r_{da} for three distances z of donor and acceptor to the mirror. The upper panel is for dipoles parallel to the mirror, the lower panel for dipoles perpendicular to the mirror. Note the logarithmic r_{da}, with dimensionless scaled values on the lower abscissa and absolute distance in nanometers on the upper abscissa for $\lambda = 628$ nm. The central colored bar indicates where various terms of the Green function dominate, and to which process.

while for the perpendicular configuration we find

$$\boldsymbol{\mu}^{\perp} \cdot \mathbf{G}_S(\mathbf{r}_a, \mathbf{r}_d, \omega) \cdot \boldsymbol{\mu}^{\perp} = \frac{\mu^2 c^2}{4\pi n^2 \omega^2} \left\{ \frac{1}{r_{da}^3} + \frac{1}{(\sqrt{r_{da}^2 + 4z^2})^3} \left(1 - 3 \frac{4z^2}{r_{da}^2 + 4z^2} \right) \right\}. \tag{20}$$

Both these static interactions depend on the donor–acceptor separation r_{da} as well as on z. In both cases the static interaction in a homogeneous medium is recovered for FRET pairs at distances to the mirror much larger than the donor–acceptor distance ($z \gg r_{da}$). The spatial dependence of the Förster transfer amplitude of equation (11) and of the FRET rate in equation (13) is hereby determined for both configurations.

5.1. FRET versus total energy transfer

In figure 2 we display the ratio of the FRET rate and the total energy-transfer rate as a function of donor–acceptor distance, for three distances z of the FRET pair to the mirror, and for both dipole configurations[11]. For the total

[11] Here we take $n = 1$ as we will do in all figures below.

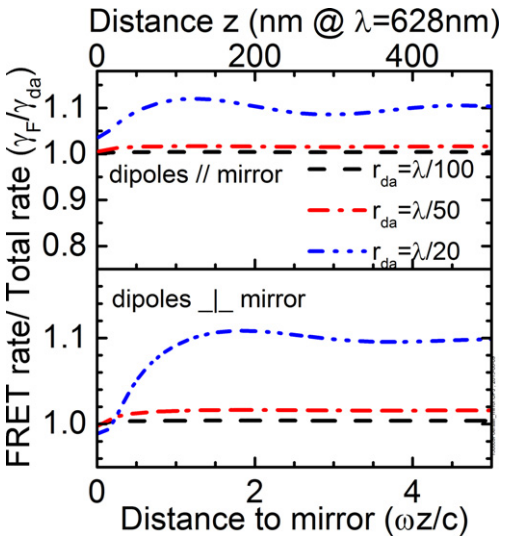

Figure 3. FRET rate γ_F divided by the total energy transfer rate γ_{da}, versus distance to the mirror, for three values of the donor–acceptor distance r_{da}. The lower abscissa is the dimensionless reduced distance, the upper abscissa is the absolute distance in nanometer for $\lambda = 628$ nm. Upper panel: parallel dipole configuration; lower panel: perpendicular dipole configuration.

rate we used the narrow bandwidth assumption of equation (4). For strongly sub-wavelength donor–acceptor distances ($r_{da}\omega/c < 0.1$), we observe that the total energy transfer rate (4) equals the FRET rate (13), irrespective of the distance to the mirror and of the dipole orientation. On a more technical level, figure 2 confirms that even in nanophotonic media, the total Green function (equation (8)) that features in the expression for energy transfer can indeed be replaced by the static Green function (equation (9)) at typical Förster-transfer distances, as was assumed in section 3.

When we increase the donor–acceptor distance beyond the Förster range ($0.1 < r_{da}\omega/c < 2$), figure 2 shows that the ratio of the two rates exceeds unity. To understand this behavior, we recall that energy transfer is proportional to the absolute value squared of the total Green function. Here, the total Green function is no longer accurately approximated by the static part. Instead, it is the sum of the static $\mathbf{G}_S$ and the radiative terms $\mathbf{G}_R$ of the total Green function (equation (8)) that has become relevant, and these two Green function terms start to interfere. For donor–acceptor distances r_{da} where the data exceed unity, the interference is destructive. The interference occurs not only near a mirror, but also for homogeneous media, as one can readily verify. As a result of the interference, one *cannot* express the total energy-transfer rate as the sum of a few partial rates, where the Förster transfer rate would be one such partial rate.

At large donor–acceptor distances ($r_{da}\omega/c \gg 1$), the FRET rate decreases much faster with distance than the total transfer rate, similar as in homogeneous media. In this distance range, the energy transfer is radiative: the donor emits a photon that is absorbed by the acceptor. Energy transfer on this larger distance scale is actively studied for various nanophotonic environments [54–59]. In contrast, in the remainder of this paper we only consider sub-wavelength donor–acceptor distances, as is the case for all FRET experiments mentioned in the Introduction. The main message of figure 2 is that for these few-nanometer distances, the total energy transfer rate (4) equals the FRET rate (13).

Figure 3 is complementary to the previous one in the sense that here the FRET rate is plotted versus distance to the mirror z for several donor–acceptor distances r_{da}, and for both dipole configurations. We again show the ratio of the FRET rate and the total transfer rate, using equation (4) for γ_{da}. At donor–acceptor distances $r_{da} = \lambda/100$ and $r_{da} = \lambda/50$, typical for experimental situations, we clearly see that FRET dominates the total energy transfer rate, independent of the distance to the mirror. At least 98% of the total energy transfer rate consists of the FRET rate. Even for a large donor–acceptor distance $r_{da} = \lambda/20$ that is much larger than in most experimental FRET cases (corresponds to $r_{da} = 31$ nm at $\lambda = 628$ nm), the FRET rate and the total rate differ by only some ten percent. Thus, figures 2 and 3 illustrate that in the nanophotonic case near an ideal mirror, the FRET dominates the total energy transfer at strongly sub-wavelength donor–acceptor distances, similar as in the well-known case of homogeneous media.

5.2. Distance-dependent transfer rate

Figure 4 shows the total energy-transfer rate between a donor and an acceptor as a function of distance z to the mirror. The panels show results for several donor–acceptor spacings $r_{da} = \lambda/100,\ \lambda/50,\ \lambda/25$. In all cases, the

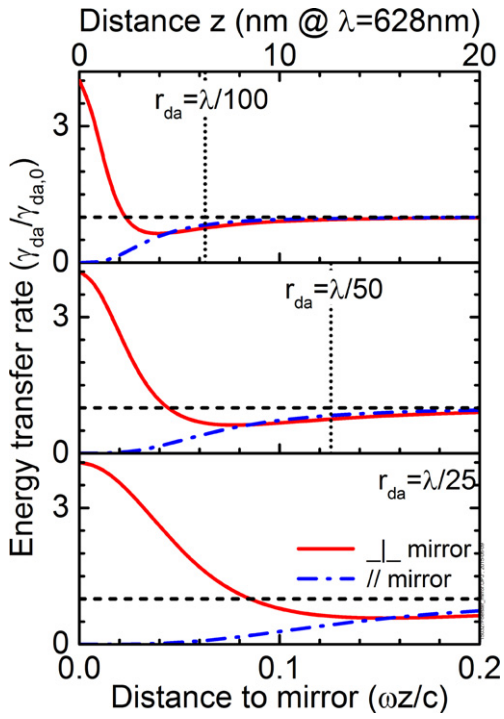

Figure 4. Total energy transfer rate between a donor and an acceptor dipole, scaled to the free-space transfer rate, versus distance to the mirror, for the parallel and perpendicular configurations. The lower abscissa gives the distance in scaled units, and the upper abscissa absolute distances at a wavelength $\lambda = (2\pi \times 100)$ nm $= 628$ nm. From top to bottom the three panels correspond to donor–acceptor spacings $r_{da} = \lambda/100,\ \lambda/50,\ \lambda/25$, where dipole-mirror distances equal to r_{da} are marked by vertical dotted lines (off scale in the lowest panel).

total energy transfer reveals a considerable z-dependence at short range. In the limit of vanishing dipole-mirror distance ($z \to 0$), dipoles perpendicular to the mirror have a four-fold enhanced transfer rate compared to free space. The factor four can be understood from the well-known method of image charges in electrodynamics: at a vanishing distance, each image dipole enhance the field two-fold, and since energy transfer invokes two dipoles, the total result is a four-fold enhancement.

With increasing dipole-mirror distance the rate in figure 4 shows a minimum at a characteristic distance that is remarkably close to the donor–acceptor spacing $z_{\min} \simeq r_{da}$. At larger distances $z > r_{da}$, the transfer rate converges to the rate in the homogeneous medium. In appendix B it is shown that this convergence holds more generally: away from surfaces or other scatterers, the FRET rate in an inhomogeneous medium is increasingly proportional to $1/(n^4 r_{da}^6)$, with n the refractive index surrounding the donor–acceptor pair.

Figure 4 also shows that in the limit of vanishing dipole-mirror distance ($z \to 0$), dipoles parallel to the mirror have an inhibited transfer rate. This result can also be understood from the method of image charges, since each image dipole reveals completely destructive interference in the limit of vanishing distance to the mirror. With increasing dipole-mirror distance z the energy-transfer rate increases monotonously, and reaches half the free-space rate at a characteristic distance that is also remarkably close to the donor–acceptor spacing $z_{1/2} \simeq r_{da}$. At larger distances $z > r_{da}$, the transfer rate tends to the homogeneous medium rate. It is remarkable that even in a simple system studied here a considerable modification of the energy transfer rate is feasible. Thus the energy transfer rate between a donor and an acceptor is controlled by the distance to the mirror, and the open question is whether this control can be understood as being mediated by the LDOS.

5.3. Energy transfer and LDOS

In figure 5, we display the distance-dependence of the energy transfer rate in comparison to the spontaneous-emission rate, over more than three orders of magnitude in distance. The spontaneous-emission rate varies with distance to the mirror on length scales comparable to the wavelength of light, as first discovered by Drexhage [40]. In contrast, the energy transfer rates vary on dramatically shorter length scales, about one-and-a-half (parallel configuration) to two (perpendicular configuration) *orders of magnitude* smaller than the wavelength scale. This result indicates that if there is a relation between energy transfer rate and LDOS, it is not a simple proportionality, as proposed in several previous studies.

To further investigate a possible relation between energy transfer rate and LDOS, figure 6 shows a parametric plot of the energy transfer rate as a function of (donor-only) spontaneous-emission rate, where each data point

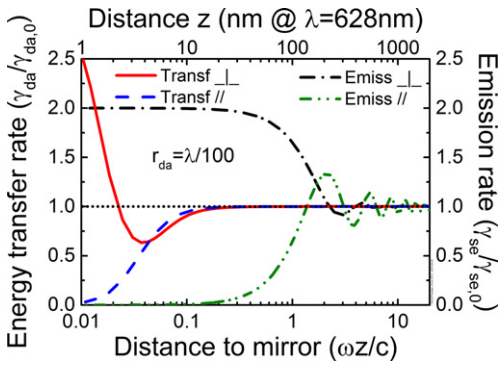

Figure 5. Comparison of donor–acceptor energy transfer rates γ_{da} and donor-only spontaneous emission rates γ_{se}, as a function of the distance z to the mirror. The lower abscissa is the scaled distance, the top abscissa is the absolute distance for $\lambda = 628$ nm, both on a log scale. The energy transfer is scaled by the free-space energy transfer rate $\gamma_{da,0}$, the spontaneous emission by the free-space rate $\gamma_{se,0}$. Data are shown both for the parallel and for the perpendicular configurations. For vanishing distance, $\gamma_{da}/\gamma_{da,0}$ is inhibited to 0 for the parallel and enhanced to 4 for the perpendicular configuration.

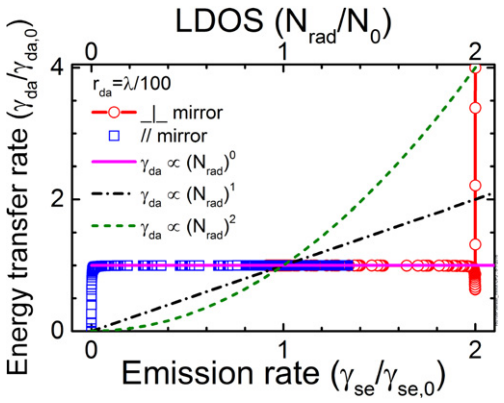

Figure 6. Parametric plot of the scaled energy transfer rate versus scaled spontaneous-emission rate (or scaled LDOS, see top abscissa) for a donor–acceptor distance $r_{da} = \lambda/100$, for dipoles perpendicular (red connected circles) and parallel (blue connected squares) to the mirror. Data are from figure 5. The magenta horizontal line shows a constant transfer rate $\gamma_{da} \propto N_{rad}^0$, the black dashed curve a linear relation $\gamma_{da} \propto N_{rad}^1$, and the green dashed curve a quadratic relation $\gamma_{da} \propto N_{rad}^2$.

pertains to a certain distance z to the mirror. The top abscissa is the relative LDOS at the donor emission frequency that equals the relative emission rate. The data at a reduced emission rate less than unity correspond mostly to the parallel dipole configurations in figures 4 and 5, whereas the results at higher emission rate correspond to mostly to the perpendicular configurations in these figures. For a typical donor–acceptor distance ($r_{da} = \lambda/100$), figure 6 shows that the energy transfer rate is independent of the emission rate and the LDOS over nearly the whole range, in agreement with conclusions of [23, 32, 34, 38]. The energy transfer decreases fast near the low emission rate edge and increases fast near the high emission rate edge, both of which correspond to distances very close to the mirror (see figure 4). From figure 6 it is readily apparent that the energy transfer rate does not increase linearly with the LDOS, leave alone quadratically, as was previously proposed.

Therefore, while both the spontaneous-emission rate and the FRET rate depend on the distance to the mirror and hence differ from the corresponding rates in a homogeneous medium, we find no position-dependent correlation between the two rates in figure 5 and no LDOS-dependent correlation in figure 6. These results are related to the absence of a frequency-dependent correlation between the two rates that we derived in section 3: if we keep the spatial positions ($\mathbf{r}_a$, $\mathbf{r}_d$) fixed while shifting the central frequencies of the donor and acceptor spectra (ω_d, ω_a) by the same frequency ($\Delta\omega$), then the spontaneous-emission rate obviously changes (see equation (5)) in response to a similar change in LDOS, whereas our equation (13) reveals that the position-dependent FRET rate remains constant.

5.4. FRET and integrated LDOS

To verify the accuracy of the LDOS-approximated FRET rate $\gamma_F^{(L)}$ near the ideal mirror, we vary the frequency bandwidth Ω over which we integrate the LDOS (see equations (17) and (18)). The required frequency integrals

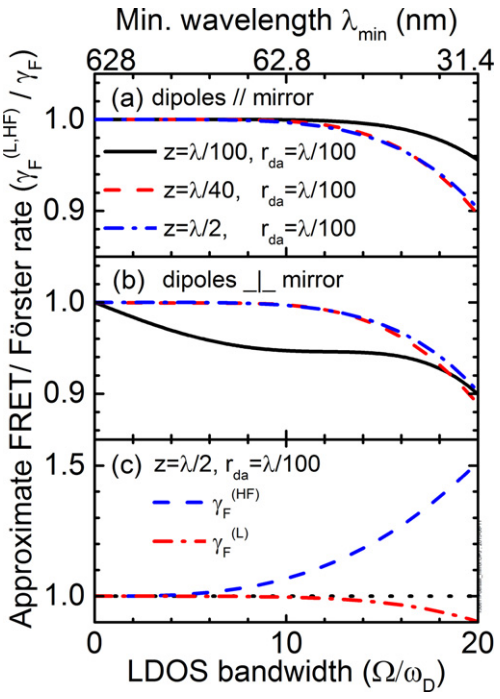

Figure 7. LDOS-approximated FRET rate $\gamma_F^{(L)}$ (equation (18)) normalized to the exact FRET rate γ_F (equation (12)) versus the bandwidth Ω of the LDOS-frequency integral. Lower abscissa: Ω scaled by the donor frequency $\omega_d = 2\pi c/\lambda$. Upper abscissa: minimum wavelength $\lambda_{min} = 2\pi c/\Omega$ for $\lambda = 628$ nm. Black full curves are for dipole-to-mirror distance $z = \lambda/100$, red dashed curves for $z = \lambda/40$, and blue dashed–dotted curves for $z = \lambda/2$, all curves are for a donor–acceptor distance $r_{da} = \lambda/100$. (a) Parallel dipole configuration; (b) perpendicular dipole configuration. (c) Comparison of the LDOS-approximation (equation (18)) and the HF approximation (equation (21)) of the FRET rate as a function of LDOS bandwidth Ω. Rates are scaled to the exact FRET rate, and the distance to the mirror and the donor–acceptor distance are fixed.

in equation (16) are calculated analytically in appendix D.2. In figure 7 we see that for both dipole configurations, the approximate FRET rate indeed tends to the exact rate for vanishing $\Omega \to 0$. For Ω up to $10\omega_d$, the approximate rate is very close to the exact one, to within 5%. At even higher frequencies, up to $\Omega = 20\omega_d$, the approximate FRET rate is within 10% of the exact rate, as anticipated in section 4 on the basis of general considerations.

The validity of the approximate FRET rate $\gamma_F^{(L)}$ improves when the donor–acceptor distance r_{da} is reduced, since the spatial zero-order Taylor expansion of Im[**G**] is then a better approximation. We can also improve the approximation by reducing the frequency bandwidth Ω in which we make the Taylor approximation. Both trends are indeed found in appendix D.1 where $\gamma_F^{(L)}$ is calculated for the homogeneous medium. In the limit of a vanishing frequency bandwidth ($\Omega \to 0$), the approximate Förster transfer rate $\gamma_F^{(L)}$ reduces to the exact Förster transfer rate γ_F of equation (12).

To verify that the approximate FRET rates shown in figure 7 were not 'lucky shots' for the chosen fixed distances to the mirror, we study in the complementary figure 8(a) the accuracy of $\gamma_F^{(L)}$ as a function of distance to the mirror z, for a constant LDOS bandwidth $\Omega = 10\omega_d$. The figure clearly shows the great accuracy of the LDOS approximation, irrespective of the distance z of the FRET pair to the ideal mirror. For a narrower bandwidth of $\Omega = 2\omega_d$, the accuracy is even better, as expected.

At this point, one might be tempted to conclude from figures 7 and 8 that the FRET rate is intimately related to an integral over the LDOS. This conclusion is too rash, however, because the corresponding approximate relation equation (18) consists of two integrals, where only one of them is an integral over the LDOS at the donor position, while the other is a high frequency (HF) integral of the imaginary part of the Green function featuring both donor and acceptor positions. Thus the relevant question becomes: what happens if we make a cruder approximation to the FRET rate by simply removing the LDOS integral? Instead of equation (16) we then use the HF approximation $\mathbf{G}_S^{(HF)}$ to the static Green function

$$\mathbf{G}_S^{(HF)}(\mathbf{r}_a, \mathbf{r}_d, \omega) = \frac{2}{\pi\omega^2}\int_\Omega^\infty d\omega_1\, \omega_1\, \mathrm{Im}[\mathbf{G}(\mathbf{r}_a, \mathbf{r}_d, \omega_1)]. \quad (21)$$

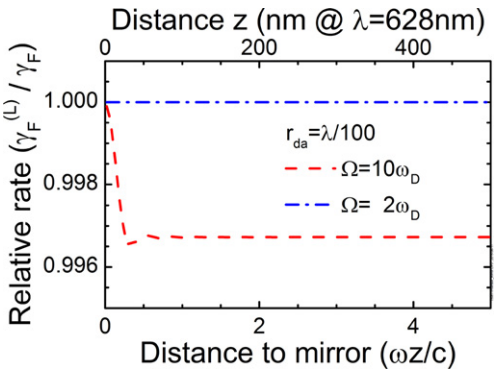

Figure 8. LDOS-approximated FRET rate $\gamma_F^{(L)}$ (equation (18)) normalized to the exact FRET rate γ_F (equation (12)) versus (scaled) distance to the mirror, for an LDOS frequency bandwidth up to $\Omega = 10\omega_0$ (red dashed curve), and up to $\Omega = 2\omega_0$ (blue dashed–dotted curve). The donor–acceptor distance is $r_{da} = \lambda/100$.

This leads to a HF approximation to the squared Förster amplitude

$$w_F^{(HF)} = (2\pi/\hbar^2)(\omega/(\varepsilon_0 c^2))^2 |\boldsymbol{\mu}_a^* \cdot \mathbf{G}_S^{(HF)}(\mathbf{r}_a, \mathbf{r}_d, \omega) \cdot \boldsymbol{\mu}_d|^2 \tag{22}$$

and a HF approximation to the FRET rate

$$\gamma_F^{(HF)} = w_F^{(HF)}(\mathbf{r}_a, \mathbf{r}_d) \int_{-\infty}^{\infty} \mathrm{d}\omega\, \sigma_a(\omega)\sigma_d(\omega), \tag{23}$$

which is independent of frequency, similar as γ_F and $\gamma_F^{(L)}$. In figure 7(c) the two approximated FRET rates $\gamma_F^{(L)}$ and $\gamma_F^{(HF)}$ are compared for the ideal mirror as a function of the bandwidth Ω, while keeping the donor–acceptor distance r_{da} and the distance to the mirror z fixed. Indeed $\gamma_F^{(L)}$ is the more accurate approximation of the two, yet $\gamma_F^{(HF)}$ is not a bad approximation at all: by only integrating in equation (23) over high frequencies $\Omega \geqslant 10\omega_d$, $\gamma_F^{(HF)}$ is accurate to within about 7%. If we take a narrower—yet still broad—frequency bandwidth, for example up to $\Omega = 2\omega_d$ (in the UV), we still neglect the LDOS in the whole visible range. Nevertheless figure 7(c) shows that for $\Omega = 2\omega_d$ the two approximations $\gamma_F^{(L)}$ and $\gamma_F^{(HF)}$ agree to a high accuracy with the exact rate γ_F. Therefore, figures 7 and 8 show that for the ideal mirror there is essentially no dependence of the FRET rate on the frequency-integrated LDOS at visible frequencies, and only a weak dependence on the frequency-integrated LDOS at UV frequencies and beyond. We note that this conclusion is complementary to the one in section 3, where the FRET rate was found not to depend on the LDOS at one frequency namely at $\hbar\omega_d$. In addition, this conclusion that the FRET rate numerically is independent from the integrated LDOS is completely consistent with our derivation that the LDOS approximation equation (17) for Förster transfer, featuring a broadband LDOS integral, is accurate.

6. Discussion

We discuss consequences of our theoretical results to experiments, first regarding relevant length scales. We have performed analytical calculations and plotted rates versus reduced lengths, namely the reduced distance to the mirror $z\omega/c = 2\pi z/\lambda$ and the reduced donor–acceptor distance r_{da}/λ. For the benefit of experiments and applications, we have plotted in several figures additional abscissae for absolute length scales that pertain to a particular choice of the donor emission wavelength λ_d. We have chosen $\lambda_d = 2\pi/\omega_d = (2\pi \times 100)$ nm $\simeq 628$ nm, a figure that we call a 'Mermin-wavelength' [63] as it simplifies the conversion between reduced units and real units to a mere 100× multiplication. Figure 2 characterizes the donor–acceptor distance dependence of the transfer rate. It is apparent that Förster transfer dominates in the range $r_{da} < 20$ nm, a length scale much smaller than the wavelength of light. Energy transfer is dominated by radiative transfer in the range $r_{da} > 100$ nm, which is reasonable as this distance range is of the order of the wavelength.

Figure 4 characterizes the distance dependence to the mirror. The range where both the total and the FRET rates are controlled by the distance to the mirror is in the range $z < 20$ nm. This range is set by the donor–acceptor distance that is for most typical FRET pairs in the order of $r_{da} = 10$ nm, in view of typical Förster distances of the same size [2]. Interestingly, while the energy transfer in this range ($z < r_{da}$) is not controlled by the LDOS, the transfer rate is nevertheless controlled by precise positioning near a mirror. An example of a method that could be used to achieve such control at optical wavelengths is by attaching emitters, such as

molecules or quantum dots, to the ends of brush polymers with sub-10 nm lengths [60]. With Rydberg atoms, it appears to be feasible to realize the situation $z < r_{da}$, albeit in the GHz frequency range [61].

How do our theoretical results compare to experiments? Our theoretical findings support the FRET-rate and spontaneous-emission rate measurements by [32], where it was observed that Förster transfer rates are not affected by the LDOS. Our findings also agree with the results of [23, 34, 36, 38]. In other experiments where a relation between FRET and LDOS was found, this could be the case if the energy transfer is not dominated by Förster energy transfer, or if the medium is strongly dispersive. Furthermore, our theory does currentely not include typical aspects of experiments, such as incompletely paired donors, cross-talk between dense donor–acceptor pairs, inhomogeneously distributed donor–acceptor distances, etcetera.

Let us turn to broadband LDOS control: in [23] qualitative arguments were given that FRET rates are a more broadband property than the LDOS, namely that the energy transfer rate is determined by the electromagnetic modes with the wave vectors of the order of $1/r_{da}$, while the density of states has contributions from all modes. Here, we have provided quantitative support for this argument by deriving the relation (equation (16)) between the static Green function and the integrated LDOS. This relation induces the new question whether FRET rates can be controlled by the broadband frequency-integrated LDOS. Since we are not aware of experiments where FRET rates are compared with frequency-integrated LDOS, we base our discussion on our present numerical results for the ideal mirror. If one wants to control the FRET rate by manipulating the LDOS, then figure 7 shows that one must control the LDOS over a huge bandwidth that ranges all the way from zero frequency ('DC') to a frequency Ω that is on the order of ten times the donor emission frequency ω_d. If we consider the Mermin-wavelength 628 nm, then the upper bound on the LDOS bandwidth corresponds to a wavelength of 63 nm, deep in the vacuum ultraviolet (VUV) range. At these very short wavelengths, all materials that are commonly used in nanophotonic control are strongly absorbing, e.g., dielectrics such as silica, semiconductors such as silicon, or metals such as silver. In practice, the optical properties of typical nanophotonic materials differ from their commonly used properties at wavelengths below 200–250 nm, which corresponds to $\Omega < 3\omega_d$. Yet, even if one were able to control the LDOS over such a phenomenally broad bandwidth $0 < \Omega < 3\omega_d$, figure 8 shows that the broadband LDOS-integral contributes negligibly—much less than 10^{-3}—to the Förster transfer rate. In brief, if the ideal mirror is exemplary for arbitrary photonic media, which we think it is, then controlling the FRET rate via the frequency-integrated LDOS seems rather unlikely.

In quantum information processing, FRET is a mechanism by which nearby (<10 nm) qubits may interact [15–20], intended or not. Lovett *et al* considered the implications of FRET between two quantum dots [17]. In one implementation, it was found that it is desirable to suppress the Förster interaction to create entanglement using biexcitons. In another implementation, it was found that FRET should not be suppressed, but switched in time. There is a growing interest in manipulating the LDOS, either suppressing it by means of a complete 3D photonic band gap [43], or by ultrafast switching in the time-domain [62]. It follows from our present results that these tools cannot be used to switch or suppress FRET between quantum bits in this way. Conversely, our results indicate that FRET-related quantum information processing may be controlled by carefully positioning the interacting quantum systems (i.e, the quantum dots) in engineered inhomogeneous dielectric environments.

7. Conclusions

Motivated by the current debate in nanophotonics about the control of FRET—notably regarding the role of the LDOS—we have studied FRET in arbitrary nanophotonic media with weak dispersion and weak absorption in the frequency overlap range of donor and acceptor. This system has allowed us to obtain two new insights.

Firstly, we investigated the dependency of the FRET rate on the Green function. We argued that for the FRET rate one only needs to consider the static part of the Green function (see equations (8) and (9)). Hence, the Förster transfer rate (equation (13)) becomes independent of frequency, in contrast to spontaneous-emission rates that are strongly frequency dependent in nanophotonic media, as mediated by the LDOS. It follows from this result that the position-dependent FRET rate and the LDOS at the donor transion frequency are completely uncorrelated for any nondispersive medium. Even for weakly dispersive media we expect this conclusion to hold.

Secondly, we derived an exact expression for the FRET rate as a frequency integral of the imaginary part of the Green function. This leads to very accurate approximation for the FRET rate in terms of a broadband frequency integral over the LDOS (equation (18)), *integrated over a huge bandwidth* from zero frequency to far into the UV, which offers a new perspective on the relation between the LDOS and the FRET rate.

Using an exactly solvable analytical model system of a donor and an acceptor near an ideal mirror, we have seen that the FRET rate differs from the FRET rate in the corresponding homogeneous medium. For two particular dipole configurations, we found that the FRET rate is inhibited ($\to 0$) or markedly enhanced (by a factor $4\times$). Thus, even this simple model system offers the opportunity to control energy transfer rates at

distances close to the mirror, typically a few nm. Nevertheless, we find that the FRET rate is independent of the LDOS at the donor emission frequency. Moreover, we observe that the FRET rate hardly depends on the frequency-integrated LDOS. It is enticing that our general result that the FRET rate and the LDOS are uncorrelated, is corroborated by the examplary system of the ideal mirror.

We also used the example of the mirror to test the approximate relation equation (16) of the FRET rate in terms of the sum of the frequency-integrated LDOS and a second integral over UV frequencies and higher. We verified that the approximation is indeed extremely accurate, as we anticipated. Remarkably, a detailed quantitative consideration reveals that the broadband LDOS-integral in equation (16) contributes negligibly to the FRET rate, while the FRET rate can be accurately approximated in terms of only the second (HF) integral, at least for the specific medium considered here. So not only can FRET rates not be controlled by changing the LDOS, as earlier theoretical and experimental work also showed, but FRET rates even seem to be practically immune to changes in the frequency-integrated LDOS as well.

As future extensions of our work, it will be interesting to study the contribution of the integrated LDOS to the approximate relation (equation (16)) for the FRET rate also for more complex photonic media, and whether such an integral relation also holds for dispersive and lossy media. Finally, we have discussed the consequences of our results to applications of Förster resonance energy transfer, for instance in quantum information processing.

Acknowledgments

It is a great pleasure to thank Bill Barnes, Christian Blum, Ad Lagendijk, Asger Mortensen, and Allard Mosk for stimulating discussions, and Bill Barnes for pointing out [63]. MW gratefully acknowledges support from the Villum Foundation via the VKR Centre of Excellence NATEC-II and from the Danish Council for Independent Research (FNU 1323-00087). The Center for Nanostructured Graphene is sponsored by the Danish National Research Foundation, Project DNRF58. WLV gratefully acknowledges support from FOM, NWO, STW, and the Applied Nanophotonics (ANP) section of the MESA+ Institute.

Appendix A. Green tensor for planar mirror

The Green tensor in a homogeneous medium with real-valued refractive index n is given by [64]

$$\begin{aligned}\mathbf{G}_{\mathrm{h}}(\mathbf{r}_1,\,\mathbf{r}_2,\,\omega) &= \mathbf{G}_{\mathrm{h}}(\mathbf{r},\,\omega)\\ &= -\frac{\mathrm{e}^{w}}{4\pi r}[P(w)\mathbf{I} + Q(w)\hat{\mathbf{r}}\otimes\hat{\mathbf{r}}] + \frac{1}{3(n\omega/c)^2}\delta(\mathbf{r})\mathbf{I},\end{aligned} \tag{A.1}$$

withe $\mathbf{r} = \mathbf{r}_1 - \mathbf{r}_2$, the functions $P,\ Q$ are defined as $P(w) \equiv (1 - w^{-1} + w^{-2})$ and $Q(w) \equiv (-1 + 3w^{-1} - 3w^{-2})$, and the argument equals $w = (\mathrm{i}n\omega r/c)$. For $n = 1$, $\mathbf{G}_{\mathrm{h}}$ equals the free-space Green function, denoted by $\mathbf{G}_0$. For distances much smaller than an optical wavelength ($r \ll \lambda = 2\pi c/(n\omega)$), the Green function scales as $\mathbf{G}_{\mathrm{h}}(\mathbf{r},\,\omega) \propto 1/(n^2r^3)$. From equations (1) and (2) we then obtain the characteristic scaling of the Förster transfer rate as $\gamma_{\mathrm{da}} \propto 1/(n^4r_{\mathrm{da}}^6)$: the Förster transfer rate strongly *decreases* with increasing donor–acceptor distance and with increasing refractive index. In contrast, it follows from equation (5) that the spontaneous-emission rate γ_{se} in a homogeneous medium is *enhanced* by a factor n compared to free space. More refined analyses that include local-field effects likewise predict a spontaneous-emission enhancement [65].

Next, we determine the Green function of an ideal flat mirror within an otherwise homogeneous medium with refractive index n. While the function can be found with various methods [45, 66], we briefly show how it is obtained by generalizing the multiple-scattering formalism of [67] for infinitely thin planes. In the usual mixed Fourier-real-space representation ($\mathbf{k}_{\|},\,z$) relevant to planar systems with translational invariance in the (x, y)-directions, the homogeneous-medium Green function $\mathbf{G}_{\mathrm{h}}(\mathbf{k}_{\|},\,z,\,z',\,\omega)$ becomes

$$\mathbf{G}_{\mathrm{h}} = \begin{pmatrix}1 & 0 & 0\\ 0 & k_z^2 & -k_{\|}k_z s_{zz'}\\ 0 & -k_{\|}k_z s_{zz'} & k_{\|}^2\end{pmatrix}\frac{c^2}{(n\omega)^2}g_{\mathrm{h}} + \frac{\delta(z-z')}{(n\omega/c)^2}\hat{\mathbf{z}}\hat{\mathbf{z}}, \tag{A.2}$$

where the scalar Green function is given by $g_{\mathrm{h}} = g_{\mathrm{h}}(\mathbf{k}_{\|},\,z,\,z',\,\omega) = \exp(2\mathrm{i}k_z|z-z'|)\,/(2\mathrm{i}k_z)$, $k_z = (n\omega^2/c^2 - k_{\|}^2)^{1/2}$, $s_{zz'} = \mathrm{sign}(z-z')$ and the matrix is represented in the basis ($\hat{\mathbf{s}}_{\mathbf{k}},\,\hat{\mathbf{p}}_{\mathbf{k}},\,\hat{\mathbf{z}}$), where $\mathbf{k}$ is the wave vector of the incoming light, $\hat{\mathbf{z}}$ is the positive-z-direction, $\hat{\mathbf{s}}_{\mathbf{k}}$ is the direction of s-polarized light (out of the plane of incidence), and $\hat{\mathbf{p}}_{\mathbf{k}}$ points perpendicular to $\hat{\mathbf{z}}$ in the plane of incidence. An infinitely thin plane at $z = 0$ that scatters light can be described by a T-matrix $\mathbf{T}(\mathbf{k}_{\|},\,\omega)$, in terms of which the Green function becomes

$$\mathbf{G}(z,\,z') = \mathbf{G}_{\mathrm{h}}(z,\,z') + \mathbf{G}_{\mathrm{h}}(z,\,0)\mathbf{T}\,\mathbf{G}_{\mathrm{h}}(0,\,z'), \tag{A.3}$$

where the $(\mathbf{k}_\parallel, \omega)$ dependence was dropped. It was found in [67] that for an infinitely thin plane that models a finite-thickness dielectric slab of dielectric constant ε, the T-matrix assumes a diagonal form in the same basis as $\mathbf{G}_\mathrm{h}$ in equation (A.2), in particular $\mathbf{T} = \mathrm{diag}(T^{\mathrm{ss}}, T^{\mathrm{pp}}, 0)$. The infinitely thin plane becomes a perfectly reflecting mirror if we choose for example a lossless Drude response with $\varepsilon = 1 - \omega_\mathrm{p}^2/\omega^2$, in the limit of an infinite plasma frequency $\omega_\mathrm{p} \to \infty$. Hence the T-matrix for a perfect mirror in a homogeneous dielectric has nonzero diagonal components $T^{\mathrm{ss}} = -2\mathrm{i}k_z$ and $T^{\mathrm{pp}} = -2\mathrm{i}(n\omega/c)^2/k_z$. The ideal mirror divides space into two optically disconnected half spaces, and below we only consider the half space $z \geqslant 0$. It then follows that the Green function for the ideal mirror is written in terms of homogeneous-medium Green functions as

$$\mathbf{G}(z, z') = \mathbf{G}_\mathrm{h}(z - z') - \mathbf{G}_\mathrm{h}(z + z') + 2\left(\frac{k_\parallel c}{n\omega}\right)^2 g_\mathrm{h}(z + z')\hat{\mathbf{z}}\hat{\mathbf{z}}, \tag{A.4}$$

where the $(\mathbf{k}_\parallel, \omega)$-dependence of the Green functions was again suppressed. To understand energy transfer rates near a mirror, we need to determine the Green function in the real-space representation, which is related to the previous equation by the inverse Fourier transform

$$\mathbf{G}(\mathbf{r}, \mathbf{r}', \omega) = \frac{1}{(2\pi)^2}\int \mathrm{d}^2\mathbf{k}_\parallel\, \mathbf{G}(\mathbf{k}_\parallel, z, z', \omega)\mathrm{e}^{\mathrm{i}\mathbf{k}_\parallel(\boldsymbol{\rho}-\boldsymbol{\rho}')}, \tag{A.5}$$

where $\boldsymbol{\rho} = (\mathbf{x}, \mathbf{y})$ and $\boldsymbol{\rho}' = (\mathbf{x}', \mathbf{y}')$ so that $\mathbf{r} = (\boldsymbol{\rho}, z)$. We find the Green function for an ideal mirror in a homogeneous medium as the sum of three terms:

$$\mathbf{G}(\mathbf{r}, \mathbf{r}', \omega) = \mathbf{G}_\mathrm{h}(\mathbf{r}, \mathbf{r}', \omega) - \mathbf{G}_\mathrm{h}(\boldsymbol{\rho}, z + z', \boldsymbol{\rho}', 0, \omega) + 2G_0^{zz}(\boldsymbol{\rho}, z + z', \boldsymbol{\rho}', 0, \omega)\hat{\mathbf{z}}\hat{\mathbf{z}}. \tag{A.6}$$

For the parallel configuration, we find

$$\boldsymbol{\mu}^\parallel \cdot \mathbf{G}(\mathbf{r}_\mathrm{a}, \mathbf{r}_\mathrm{d}, \omega) \cdot \boldsymbol{\mu}^\parallel = -\mu^2\frac{\mathrm{e}^{\mathrm{i}n\omega r_\mathrm{da}/c}}{4\pi r_\mathrm{da}}P(\mathrm{i}n\omega r_\mathrm{da}/c) + \mu^2\frac{\mathrm{e}^{\mathrm{i}n\omega u/c}}{4\pi u}P(\mathrm{i}n\omega u/c), \tag{A.7}$$

where r_da is the donor–acceptor distance, z the distance of both dipoles to the mirror, and $u \equiv [r_\mathrm{da}^2 + (2z)^2]^{1/2}$, and $\boldsymbol{\mu}^\parallel = \mu\hat{\mathbf{y}}$ as in figure 1.

For the perpendicular configuration we find

$$\boldsymbol{\mu}^\perp \cdot \mathbf{G}(\mathbf{r}_\mathrm{a}, \mathbf{r}_\mathrm{d}, \omega) \cdot \boldsymbol{\mu}^\perp = -\mu^2\frac{\mathrm{e}^{\mathrm{i}n\omega r_\mathrm{da}/c}}{4\pi r_\mathrm{da}}P(\mathrm{i}n\omega r_\mathrm{da}/c) - \mu^2\frac{\mathrm{e}^{\mathrm{i}n\omega u/c}}{4\pi u}\left[P(\mathrm{i}n\omega u/c) + 4\left(\frac{z}{u}\right)^2 Q(\mathrm{i}n\omega u/c)\right], \tag{A.8}$$

with $\boldsymbol{\mu}^\perp = \mu\hat{\mathbf{z}}$ as in figure 1 and u as in equation (A.7).

For completeness, we also give the known [66] single-emitter spontaneous-emission rates near the mirror (neglecting local-field effects [65] here and below). For a dipole at a distance z oriented parallel to the mirror, we find from equations (5) and (A.6)

$$\gamma_\mathrm{se}^\parallel(z, \omega) = \gamma_\mathrm{se,h}(\omega)\left\{1 - \frac{3}{2}\left[\frac{\sin(\alpha)}{\alpha} + \frac{\cos(\alpha)}{\alpha^2} - \frac{\sin(\alpha)}{\alpha^3}\right]\right\}, \tag{A.9a}$$

in terms of $\alpha = 2n\omega z/c$ and the homogeneous-medium spontaneous-emission rate $\gamma_\mathrm{se,h} = \mu^2 n\omega^3/(3\pi\hbar\varepsilon_0 c^3)$, i.e, n times the spontaneous-emission rate in free space. For a dipole emitter oriented normal to the mirror, the position-dependent spontaneous emission rate becomes

$$\gamma_\mathrm{se}^\perp(z, \omega) = \gamma_\mathrm{se,h}(\omega)\left\{1 - 3\left[\frac{\cos\alpha}{\alpha^2} - \frac{\sin\alpha}{\alpha^3}\right]\right\}. \tag{A.9b}$$

In the limit $z \to 0$, the rate $\gamma_\mathrm{se}^\parallel(z, \omega)$ vanishes, while $\gamma_\mathrm{se}^\perp(z, \omega)$ tends to $2\gamma_\mathrm{se,h}$. In the limit $z \to \infty$, both $\gamma_\mathrm{se}^\parallel(z, \omega)$ and $\gamma_\mathrm{se}^\perp(z, \omega)$ tend to the homogeneous-medium rate $\gamma_\mathrm{se,h}(\omega)$.

Appendix B. Scaling with donor–acceptor distance of Förster transfer rate

Here we show that the homogeneous-medium Förster transfer rate, scaling as $\propto 1/(n_\mathrm{h}^4 r_\mathrm{da}^6)$, is an important limiting case also for inhomogeneous media. Let us assume that the donor and acceptor are separated by a few nanometer, experiencing the same dielectric material with a dielectric function ε_h, within an inhomogeneous nanophotonic environment. In all of space, we define the optical potential $\mathbf{V}(\mathbf{r}, \omega) = -[\varepsilon(\mathbf{r}) - \varepsilon_\mathrm{h}](\omega/c)^2\mathbf{I}$, so that the optical potential vanishes in the vicinity of the donor–acceptor pair. Then the Green function of the medium can be expressed in terms of the homogeneous-medium Green function and the optical potential as

$$\mathbf{G}(\mathbf{r}_\mathrm{a}, \mathbf{r}_\mathrm{d}, \omega) = \mathbf{G}_\mathrm{h}(\mathbf{r}_\mathrm{a} - \mathbf{r}_\mathrm{d}, \omega) + \int \mathrm{d}\mathbf{r}_1\, \mathbf{G}_\mathrm{h}(\mathbf{r}_\mathrm{a} - \mathbf{r}_1, \omega) \cdot \mathbf{V}(\mathbf{r}_1, \omega) \cdot \mathbf{G}(\mathbf{r}_1, \mathbf{r}_\mathrm{d}, \omega), \tag{B.1}$$

which is the Dyson–Schwinger equation for the Green function that controls the energy transfer. The equation can be formally solved in terms of the T-matrix of the medium as

$$\mathbf{G}(\mathbf{r}_a, \mathbf{r}_d) = \mathbf{G}_h(\mathbf{r}_a - \mathbf{r}_d) + \int d\mathbf{r}_1 d\mathbf{r}_2\, \mathbf{G}_h(\mathbf{r}_a - \mathbf{r}_1) \cdot \mathbf{T}(\mathbf{r}_1, \mathbf{r}_2) \cdot \mathbf{G}_h(\mathbf{r}_2 - \mathbf{r}_D), \tag{B.2}$$

where the frequency dependence was dropped for readability. The important property of the T-matrix $\mathbf{T}(\mathbf{r}_1, \mathbf{r}_2, \omega)$ is now that it is only non-vanishing where both $\mathbf{V}(\mathbf{r}_1)$ and $\mathbf{V}(\mathbf{r}_2)$ are nonzero, so that it vanishes in the vicinity of the donor–acceptor pair. Thus the Green function that controls the energy transfer is given by a homogeneous-medium Green function and a scattering term. The former is a function of the distance between donor and acceptor, whereas the latter does not depend on the D–A distance, but rather on the distance of donor and acceptor to points in space where the optical potential is non-vanishing.

As the donor–acceptor distance r_{da} is decreased, the homogeneous-medium contribution in equation (B.2) grows rapidly, essentially becoming equal to $\mathbf{G}_{h,S}(\mathbf{r}_a - \mathbf{r}_d, \omega)$ of equation (10), whereas the contribution of the scattering term does not change much. So in the limit of very small r_{da}, or when making the distance to interfaces larger, the homogeneous-medium term always wins, and one would find the well-known Förster transfer rate of the infinite homogeneous medium $\propto 1/(n_h^4 r_{da}^6)$.

Appendix C. Tests of identity (15)

C.1. Test for a homogeneous medium

The Green function $\mathbf{G}_h(\mathbf{r}, \omega)$ for homogeneous media is given in equation (A.1), and its static part by equation (10). The identity (15) that relates them can be shown to hold as a tensorial identity; here we derive the identity for its projection $\boldsymbol{\mu} \cdot \mathbf{G}_h(\mathbf{r}, \omega) \cdot \boldsymbol{\mu}$, where we assume $\boldsymbol{\mu}$ to be perpendicular to $\mathbf{r}$. (Physically, this corresponds to energy transfer between donor and acceptor with equal dipoles both pointing perpendicular to their position difference vector.) The projection of the identity (15) that we are to derive has the form

$$\frac{\mu^2 c^2}{4\pi n^2 \omega^2} \frac{1}{r_{da}^3} = \frac{\mu^2}{2\pi^2 n^2 \omega^2} \frac{1}{r_{da}} \int_0^\infty d\omega_1 \omega_1 \mathrm{Im}[e^{in\omega r_{da}/c} P(in\omega r_{da}/c)]. \tag{C.1}$$

Now by integration variable transformation the right-hand side of this equation can be worked out to give

$$\frac{\mu^2 c^2}{2\pi^2 n^2 \omega^2 r_{da}^3} \int_0^\infty dx \left[\cos(kx) + x \sin(kx) - \frac{\sin(x)}{x} \right], \tag{C.2}$$

with dummy variable k equal to unity. Now the first two terms within the square brackets do not contribute to the integral since $\int_0^\infty dx \cos(kx) = \pi\delta(k)$ and $\int_0^\infty dx\, x \sin(kx) = -\pi \frac{d}{dk}\delta(k)$, while the third term in the square brackets of equation (C.2) does contribute since $\int_0^\infty dx \sin(x)/x = \pi/2$. Thus the projection of the identity (15) indeed holds for spatially homogeneous media.

C.2. Test for an ideal mirror

For the ideal mirror we again only consider a projection of the identity (15), first projecting onto dipoles corresponding to the parallel configuration of figure 1. The Green function for the ideal mirror is given in equation (A.6), and its static part for the parallel configuration by equation (19). Now for this parallel configuration, the projected Green tensor consists of a homogeneous-medium and a reflected part, and so does the projected static Green function. In section C.1 above we already showed that the sought identity indeed holds for homogeneous media. So the remaining task is to show that the identity (15) holds separately for the reflected parts of the projected Green functions. This is not difficult since mathematically the frequency integral that is to be performed is the same as for the homogeneous medium; only the distance parameter r_{da} is to be replaced by $\sqrt{r_{da}^2 + 4z^2}$. Thus the projection of the identity (15) onto the parallel dipole directions indeed holds. The qualitative novelty as compared to the homogeneous-medium case is that we thus show that the identity holds irrespective of the distance z of the FRET pair to the mirror. We also checked (not shown) that the identity (15) holds for the projection onto perpendicular dipoles, i.e. as in the perpendicular configuration of figure 1.

Appendix D. Accuracy of the approximate expressions (16) and (23)

To test the accuracy of the LDOS approximation $\mathbf{G}_S^{(L)}(\mathbf{r}_a, \mathbf{r}_d, \omega)$ of the static Green function, it is convenient to use equation (15) to rewrite equation (16) as

$$\mathbf{G}_S^{(L)}(\mathbf{r}_a, \mathbf{r}_d, \omega) = \mathbf{G}_S(\mathbf{r}_a, \mathbf{r}_d, \omega) + \frac{2}{\pi\omega^2} \int_0^\Omega d\omega_1\, \omega_1\, \mathrm{Im}[\mathbf{G}(\mathbf{r}_d, \mathbf{r}_d, \omega_1) - \mathbf{G}(\mathbf{r}_a, \mathbf{r}_d, \omega_1)], \tag{D.1}$$

In this form, the approximate static Green function is equal to the exact expression plus an integral over a finite interval of a well-behaved integrand. Likewise, to test the accuracy of the HF approximation $\mathbf{G}_S^{(HF)}(\mathbf{r}_a, \mathbf{r}_d, \omega)$ defined in equation (23) of the static Green function, it is useful to rewrite it as

$$\mathbf{G}_{\mathrm{S}}^{(\mathrm{HF})}(\mathbf{r}_{\mathrm{a}},\,\mathbf{r}_{\mathrm{d}},\,\omega)=\mathbf{G}_{\mathrm{S}}(\mathbf{r}_{\mathrm{a}},\,\mathbf{r}_{\mathrm{d}},\,\omega)-\frac{2}{\pi\omega^2}\int_0^{\Omega}\mathrm{d}\omega_1\,\omega_1\,\mathrm{Im}[\mathbf{G}(\mathbf{r}_{\mathrm{a}},\,\mathbf{r}_{\mathrm{d}},\,\omega_1)],\tag{D.2}$$

Again the integrand is well-defined, i.e, non-diverging over the entire finite integration interval.

D.1. Accuracy of LDOS approximation for homogeneous media

We estimate the accuracy of equation (D.1) for the Green function (A.1) of a homogeneous medium. By taking the projection onto dipole vectors both on the left and right, we find

$$\mathrm{Im}\int_0^{\Omega}\mathrm{d}\omega_1\,\omega_1\,\boldsymbol{\mu}\cdot[\mathbf{G}_{\mathrm{h}}(\mathbf{r}_{\mathrm{d}},\,\mathbf{r}_{\mathrm{d}},\,\omega_1)-\mathbf{G}_{\mathrm{h}}(\mathbf{r}_{\mathrm{a}},\,\mathbf{r}_{\mathrm{d}},\,\omega_1)]\cdot\boldsymbol{\mu}=-\frac{\mu^2 n}{4\pi c}\int_0^{\Omega}\mathrm{d}\omega_1\omega_1^2\left[\frac{2}{3}-h(D)\right],\tag{D.3}$$

where $D=n\omega d/c$ and for convenience we defined the function $h(x)\equiv\cos(x)/x^2+\sin(x)(1-1/x^2)/x$. So here (and also for the mirror below) we must determine integrals of the type

$$\begin{aligned}H(\Omega,\,a)&=\int_0^{\Omega}\mathrm{d}\omega_1\omega_1^2 h(\omega_1 a)\\&=(\Omega/A)^3[\sin(A)-A\cos(A)-\mathrm{Si}(A)],\end{aligned}\tag{D.4}$$

where $A=\Omega a$ and $\mathrm{Si}[x]=\int_0^x\mathrm{d}t\,\sin(t)/t$ is the sine integral. For $\Omega a\ll 1$ we find the approximation

$$H(\Omega,\,a)=\frac{2}{9}\Omega^3-\frac{2}{75}\frac{(\Omega a)^5}{a^3}.\tag{D.5}$$

With this result, we find that the relative error of making the LDOS approximation $\mathbf{G}_{\mathrm{h,S}}^{(\mathrm{L})}(\mathbf{r}_{\mathrm{a}},\,\mathbf{r}_{\mathrm{d}},\,\omega)$ of equation (D.1) for the Green function $\mathbf{G}_{\mathrm{h,S}}(\mathbf{r}_{\mathrm{a}},\,\mathbf{r}_{\mathrm{d}},\,\omega)$ is

$$\frac{\boldsymbol{\mu}\cdot(\mathbf{G}_{\mathrm{h,S}}^{(\mathrm{L})}-\mathbf{G}_{\mathrm{h,S}})\cdot\boldsymbol{\mu}}{\boldsymbol{\mu}\cdot\mathbf{G}_{\mathrm{h,S}}\cdot\boldsymbol{\mu}}=-\frac{4}{75\pi}(n\Omega r_{\mathrm{da}}/c)^5.\tag{D.6}$$

This fifth-power dependence shows that for homogeneous media the LDOS approximation is excellent as long as $n\Omega r_{\mathrm{da}}/c\ll 1$, which for typical Förster distances of a few nanometers corresponds to a frequency bandwidth Ω of order $10\omega_{\mathrm{d}}$ in which the LDOS approximation can be made, where ω_{d} is a typical optical frequency (e.g., the donor emission frequency).

D.2. Accuracy of LDOS approximation for the ideal mirror

For the *parallel configuration* near the ideal mirror, we find equation (D.3), but with the integrand on the right-hand side replaced by

$$-\frac{\mu^2 n}{4\pi c}\omega_1^2\left\{\left[\frac{2}{3}-h(D_1)\right]-[h(2Z_1)-h(U_1)]\right\},\tag{D.7}$$

where $D_1=n\omega_1 r_{\mathrm{da}}/c$, $Z_1=n\omega_1 z/c$, and $U_1=\sqrt{D_1^2+4Z_1^2}$. So we can identify both a homogeneous-medium and a scattering contribution between the curly brackets. By threefold use of the identity (D.4) it then follows that $\boldsymbol{\mu}\cdot(\mathbf{G}_{\mathrm{S}}^{(\mathrm{L})}-\mathbf{G}_{\mathrm{S}})\cdot\boldsymbol{\mu}$ equals

$$-\frac{\mu^2 n}{2\pi^2\omega^2 c}\left\{\left[\frac{2}{9}\Omega^3-H\left(\Omega,\,\frac{nr_{\mathrm{da}}}{c}\right)\right]-\left[H\left(\Omega,\,\frac{2nz}{c}\right)-H\left(\Omega,\,\frac{nu}{c}\right)\right]\right\},\tag{D.8}$$

where $u=\sqrt{r_{\mathrm{da}}^2+4z^2}$.

For the *perpendicular configuration* near the ideal mirror, it can be found that the integrand of equation (D.3) is instead replaced by the slightly longer expression

$$rcl-\frac{\mu^2 n}{4\pi c}\omega_1^2\left\{\left(\frac{2}{3}-2h(2Z_1)+2\frac{\sin(2Z_1)}{2Z_1}\right)-h(D_1)-h(U_1)-\frac{4z^2}{\sqrt{r_{\mathrm{da}}^2+4z^2}}\left[2\frac{\sin(U_1)}{U_1}-3h(U_1)\right]\right\}.\tag{D.9}$$

The frequency integral can again be performed using the identity (D.4) and a standard integral of the type $\int\mathrm{d}x\,x\sin(x)$. The resulting expression for $\boldsymbol{\mu}\cdot(\mathbf{G}_{\mathrm{S}}^{(\mathrm{L})}-\mathbf{G}_{\mathrm{S}})\cdot\boldsymbol{\mu}$, and the corresponding result (D.8) for the parallel configuration are both used in figures 7 and 8.

References

[1] Förster T 1948 Zwischenmolekulare energiewanderung und fluoreszenz *Ann. Phys.* **437** 55

[2] Lakowicz J R 2006 *Principles of Fluorescence Spectroscopy* (Berlin: Springer)

[3] van Grondelle R, Dekker J P, Gillbro T and Sundström V 1994 Energy transfer and trapping in photosynthesis *Biochim. Biophys. Acta Bioenerg.* **1187** 1

[4] Scholes G D 2003 Long-range resonance energy transfer in molecular systems *Ann. Rev. Phys. Chem.* **54** 57

[5] Chanyawadee S, Harley R T, Henini M, Talapin D V and Lagoudakis P G 2009 Photocurrent enhancement in hybrid nanocrystal quantum-dot p–i–n photovoltaic devices *Phys. Rev. Lett.* **102** 077402
[6] Buhbut S, Itzhakov S, Tauber E, Shalom M, Hod I, Geiger T, Garini Y, Oron D and Zaban A 2010 Built-in quantum dot antennas in dye-sensitized solar cells *ACS Nano* **4** 1293
[7] Baldo M A, Thompson M E and Forrest S R 2000 High-efficiency fluorescent organic light-emitting devices using a phosphorescent sensitizer *Nature* **403** 750
[8] Vohra V, Calzaferri G, Destri S, Pasini M, Porzio W and Botta C 2010 Toward white light emission through efficient two-step energy transfer in hybrid nanofibers *ACS Nano* **4** 1409
[9] Itskos G, Othonos A, Choulis S A and Iliopoulos E 2015 Förster resonant energy transfer from an inorganic quantum well to a molecular material: unexplored aspects, losses, and implications to applications *J. Chem. Phys.* **143** 214701
[10] Medintz I L, Clapp A R, Mattoussi H, Goldman E R, Fisher B and Mauro J M 2003 Self-assembled nanoscale biosensors based on quantum dot FRET donors *Nat. Mater.* **2** 630
[11] Stryer L 1978 Fluorescence energy transfer as a spectroscopic ruler *Ann. Rev. Biochem.* **47** 819
[12] Schuler B, Lipman E A and Eaton W A 2002 Probing the free-energy surface for protein folding with single-molecule fluorescence spectroscopy *Nature* **419** 743
[13] García-Parajó M F, Hernando J, Mosteiro G S, Hoogenboom J P, van Dijk E M H P and van Hulst N F 2005 Energy transfer in single-molecule photonic wires *Chem. Phys. Chem.* **6** 819
[14] Carriba P *et al* 2008 Detection of heteromerization of more than two proteins by sequential BRET–FRET *Nat. Methods* **5** 727
[15] John S and Wang J 1991 Quantum optics of localized light in a photonic band gap *Phys. Rev.* B **43** 12772
[16] Barenco A, Deutsch D, Ekert A and Jozsa R 1995 Conditional quantum dynamics and logic gates *Phys. Rev. Lett.* **74** 4083
[17] Lovett B W, Reina J H, Nazir A and Briggs G A D 2003 Optical schemes for quantum computing in quantum dot molecules *Phys. Rev.* B **68** 205319
[18] Reina J H, Beausoleil R G, Spiller T P and Munro W J 2004 Radiative corrections and quantum gates in molecular systems *Phys. Rev. Lett.* **93** 250501
[19] Nazir A, Lovett B W, Barrett S D, Reina J H and Briggs G A D 2005 Anticrossings in Förster coupled quantum dots *Phys. Rev.* B **71** 045334
[20] Unold T, Mueller K, Lienau C, Elsaesser T and Wieck A D 2005 Optical control of excitons in a pair of quantum dots coupled by the dipole–dipole interaction *Phys. Rev. Lett.* **94** 137404
[21] Andrew P and Barnes W L 2000 Förster energy transfer in an optical microcavity *Science* **290** 785
[22] Dung H T, Knöll L and Welsch D-G 2002 Intermolecular energy transfer in the presence of dispersing and absorbing media *Phys. Rev.* A **65** 043813
[23] de Dood M J A, Knoester J, Tip A and Polman A 2005 Förster transfer and the local optical density of states in erbium-doped silica *Phys. Rev.* B **71** 115102
[24] Nakamura T, Fujii M, Imakita K and Hayashi S 2005 Modification of energy transfer from Si nanocrystals to Er^{3+} near a Au thin film *Phys. Rev.* B **72** 235412
[25] Nakamura T, Fujii M, Miura S, Inui M and Hayashi S 2006 Enhancement and suppression of energy transfer from Si nanocrystals to Er ions through a control of the photonic mode density *Phys. Rev.* B **74** 045302
[26] Govorov A O, Lee J and Kotov N A 2007 Theory of plasmon-enhanced Förster energy transfer in optically excited semiconductor and metal nanoparticles *Phys. Rev.* B **76** 125308
[27] Kolaric B, Baert K, van der Auweraer M, Vallée R A L and Clays K 2007 Controlling the fluorescence resonant energy transfer by photonic crystal band gap engineering *Chem. Mater.* **19** 5547
[28] Yang Z W, Zhou X R, Huang X G, Zhou J, Yang G, Xie Q, Sun L and Li B 2008 Energy transfer between fluorescent dyes in photonic crystals *Opt. Lett.* **33** 1963
[29] Xie H Y, Chung H Y, Leung P T and Tsai D P 2009 Plasmonic enhancement of Förster energy transfer between two molecules in the vicinity of a metallic nanoparticle: nonlocal optical effects *Phys. Rev.* B **80** 155448
[30] Pustovit V N and Shahbazyan T V 2011 Resonance energy transfer near metal nanostructures mediated by surface plasmons *Phys. Rev.* B **83** 085427
[31] Velizhanin K A and Shahbazyan T V 2012 Long-range plasmon-assisted energy transfer over doped graphene *Phys. Rev.* B **86** 245432
[32] Blum C, Zijlstra N, Lagendijk A, Wubs M, Mosk A P, Subramaniam V and Vos W L 2012 Nanophotonic control of the Förster resonance energy transfer efficiency *Phys. Rev. Lett.* **109** 203601
[33] Gonzaga-Galeana J A and Zurita-Sánchez J R 2013 A revisitation of the Förster energy transfer near a metallic spherical nanoparticle: (1) Efficiency enhancement or reduction? (2) The control of the Förster radius of the unbounded medium. (3) The impact of the local density of states *J. Chem. Phys.* **139** 244302
[34] Rabouw F T, den Hartog S A, Senden T and Meijerink A 2014 Photonic effects on the Förster resonance energy transfer efficiency *Nat. Commun.* **5** 3610
[35] Ghenuche P, de Torres J, Moparthi S B, Grigoriev V and Wenger J 2014 Nanophotonic enhancement of the Förster resonance energy-transfer rate with single nanoapertures *Nano Lett.* **14** 4707
[36] Tumkur T U, Kitur J K, Bonner C E, Poddubny A N, Narimanov E E and Noginov M A 2015 Control of Förster energy transfer in the vicinity of metallic surfaces and hyperbolic metamaterials *Faraday Discuss.* **178** 395
[37] Poddubny A N 2015 Collective Förster energy transfer modified by a planar metallic mirror *Phys. Rev.* B **92** 155418
[38] Konrad A, Metzger M, Kern A M, Brecht M and Meixner A J 2015 Controlling the dynamics of Förster resonance energy transfer inside a tunable sub-wavelength Fabry–Pérot-resonator *Nanoscale* **7** 10204
[39] de Torres J, Ghenuche P, Moparthi S B, Grigoriev V and Wenger J 2015 FRET enhancement in aluminum zero-mode waveguides *Chem. Phys. Chem.* **16** 782
[40] Drexhage K H 1970 Influence of a dielectric interface on fluorescence decay time *J. Lumin.* **1-2** 693
[41] Sprik R, van Tiggelen B A and Lagendijk A 1996 Optical emission in periodic dielectrics *Europhys. Lett.* **35** 265
[42] Barnes W L 1998 Fluorescence near interfaces: the role of photonic mode density *J. Mod. Opt.* **45** 661
[43] Leistikow M D, Mosk A P, Yeganegi E, Huisman S R, Lagendijk A and Vos W L 2011 Inhibited spontaneous emission of quantum dots observed in a 3D photonic band gap *Phys. Rev. Lett.* **107** 193903
[44] Novotny L and Hecht B 2012 *Principles of Nano-Optics* 2nd edn (Cambridge: Cambridge University Press)
[45] Chance R R, Prock A and Silbey R 1978 Molecular fluorescence and energy transfer near interfaces *Adv. Chem. Phys.* **37** 65
[46] May V and Kühn O 2000 *Charge and Energy Transfer Dynamics in Molecular Systems* (Berlin: Wiley)

[47] Daniels G J, Jenkins R D, Bradshaw D S and Andrews D L 2003 Resonance energy transfer: the unified theory revisited *J. Chem. Phys.* **119** 2264
[48] Bohren C F and Huffman D R 1983 *Absorption and Scattering of Light by Small Particles* (New York: Wiley) ch 9
[49] Wubs M, Suttorp L G and Lagendijk A 2004 Multiple-scattering approach to interatomic interactions and superradiance in inhomogeneous dielectrics *Phys. Rev.* A **70** 053823
[50] Craig D P and Thirunamachandran T 1984 *Molecular Quantum Electrodynamics* (London: Academic)
[51] Andrews D L 1989 A unified theory of radiative and radiationless molecular energy transfer *Chem. Phys.* **135** 195
[52] Wubs M, Suttorp L G and Lagendijk A 2003 Multipole interaction between atoms and their photonic environment *Phys. Rev.* A **68** 013822
[53] Vos W L, Koenderink A F and Nikolaev I S 2009 Orientation-dependent spontaneous emission rates of a two-level quantum emitter in any nanophotonic environment *Phys. Rev.* A **80** 053802
[54] de Roque P M, van Hulst N F and Sapienza R 2015 Nanophotonic boost of intermolecular energy transfer *New J. Phys.* **17** 113052
[55] Bian T, Chang R and Leung P T 2016 Förster energy transfer between molecules in the vicinity of graphene-coated nanoparticles *Plasmonics* (doi:10.1007/s11468-015-0167-0)
[56] Bouchet D, Cao D, Carminati R, De Wilde Y and Krachmalnicoff V 2016 Long-range plasmon-assisted energy transfer between fluorescent emitters *Phys. Rev. Lett.* **116** 037401
[57] Karanikolas V D, Marocico C A and Bradley A L 2016 Tunable and long-range transfer efficiency through a graphene nanodisk *Phys. Rev.* B **93** 035426
[58] Cortes C L and Jacob Z 2016 Super-Coulombic atom–atom interactions in hyperbolic media arXiv:1601.04013v1
[59] Poudel A, Chen X and Ratner M A 2016 Enhancement of resonant energy transfer due to evanescent-wave from the metal *J. Phys. Chem. Lett.* **7** 955
[60] Schulz A S, Benetti E M, Grishina D A, Hemphenius M, Huskens J, Vancsö G J and Vos W L 2014 Polymer brushes for tunable quantum dot positioning in photonic crystals *Chemistry as Innovating Science* (*CHAINS2014*) *conf.* (*Veldhoven, The Netherlands*) (poster MN-99, www.chains2014.nl)
[61] Ravets S, Labuhn H, Barredo D, Béguin L, Lahaye T and Browaeys A 2014 Coherent dipole–dipole coupling between two single Rydberg atoms at an electrically-tuned Förster resonance *Nat. Phys.* **10** 914
[62] Thyrrestrup H, Hartsuiker A, Gérard J-M and Vos W L 2013 Non-exponential spontaneous emission dynamics for emitters in a time-dependent optical cavity *Opt. Express* **21** 23130
[63] Mermin proposed to redefine the English foot, so that the speed of light in vacuum is equal to one foot per nanosecond, see: N.D. Mermin *It's about Time: Understanding Einstein's Relativity* (Princeton University Press: Princeton NJ, 2005) p 22
[64] de Vries P, van Coevorden D V and Lagendijk A 1998 Point scatterers for classical waves *Rev. Mod. Phys.* **70** 447
[65] Schuurmans F J P, de Lang D T N, Wegdam G H, Sprik R and Lagendijk A 1998 Local-field effects on spontaneous emission in a dense supercritical gas *Phys. Rev. Lett.* **80** 5077
[66] Matloob R 2000 Radiative properties of an atom in the vicinity of a mirror *Phys. Rev.* A **62** 022113
[67] Wubs M, Suttorp L G and Lagendijk A 2004 Spontaneous-emission rates in finite photonic crystals of plane scatterers *Phys. Rev.* E **69** 016616